Combustion and Flame 239 (2022) 111816

Contents lists available at ScienceDirect

Combustion and Flame

journal homepage: www.elsevier.com/locate/combustflame

Outwardly growing premixed flames in turbulent media

Shikhar Mohan*, Moshe Matalon

Department of Mechanical Science and Engineering University of Illinois at Urbana-Champaign, Urbana, IL 61820, USA

ARTICLE INFO

Article history:
Received 12 June 2021
Revised 9 October 2021
Accepted 15 October 2021
Available online 10 November 2021

Keywords:
Expanding flames
Turbulent premixed flames
Darrieus-Landau instability
Turbulent flame speed
Flame stretch
Curvature
Hydrodynamic-strain

ABSTRACT

The propagation of outwardly expanding premixed flames in turbulent media is examined within the context of the hydrodynamic theory wherein the flame, treated as a surface of density discontinuity separating fresh combustible mixture from burned products, is propagating at a speed dependent upon local geometric and mixture/flow characteristics. An embedded manifold approach, one adept at handling multi-valued and disjointed surfaces which are frequently observed in real flames, is used to couple the flow and flame evolution. A sensitivity analysis, based on mixtures with different Markstein numbers, is performed to investigate early flame kernel development in addition to its long-term evolution. The focus is to understand the effect of turbulent flow characteristics, distinguished by the intensity of velocity fluctuations and its integral length scale, in addition to intrinsic flame instabilities (predominantly the Darrieus-Landau instability) on flame propagation. The overarching objective is to quantify their influence on the flame morphology and burning rate and to construct scaling laws for the turbulent flame speed through appropriate modifications of Damköhler's first hypothesis. Flame-turbulence interactions are inferred from statistical quantities based on its developing flame topology, including local flame curvature and hydrodynamic strain, and their combined effects integrated into the flame stretch rate experienced by the flame and the local flame speed deviation from the laminar flame speed.

1. Introduction

Characterizing turbulent flame propagation is one of the more challenging problems in current combustion research. A substantial body of literature, reviewed for example in [1–8] and references therein, is devoted to accumulating data for a number of different flow conditions and geometries. Despite this, there remains a great degree of uncertainty and variability in defining basic quantities. Primitive measures, such as the turbulent flame speed, exhibit significant scatter and demonstrate a strong dependence on geometry and even measurement approach. Deriving universal correlations in terms of flow and combustion parameters therefore remain a non-trivial exercise and as of yet, a problem of great interest in combustion theory.

The turbulent flame speed, or burning velocity, S_T is a physically meaningful quantity with many design implications, for instance in determining the mean fuel consumption rate in a combustion chamber where conditions are often, by and large, turbulent. There is a great deal of interest in constructing a unified scaling description, at least under flow conditions that have statistically well defined characteristics such as those associated with homogeneous isotropic turbulence, and for canonical configurations. Unlike the laminar burning velocity S_L, which is a purely thermodynamic property and unique to a specific mixture, turbulent flame speed data has shown a large scatter affected strongly by geometrical/flow conditions and measurement approach. A large effort, comprising of analytical [9–16], experimental [17–24], and computational [25–29] studies, has been dedicated to quantify the extent to which turbulence enhances the flame propagation and to correlate the flame propagation speed with flow properties.

Damköhler's first hypothesis has fundamentally influenced the concept of the turbulent flame speed and its scaling. Damköhler [30] postulated that a turbulent flame is an ensemble of small flame segments, each propagating at the laminar flame speed S_L. The projection of the turbulent flame surface A meanwhile is said to propagate at S_T and by equating the mass fluxes through the flame, the following expression can be obtained for the turbulent flame speed

$$S_T/S_L = A_T/A, \tag{1}$$

where A_T is the surface area of the corrugated turbulent flame. This expression shows that variations in turbulent flame speed are proportional to changes in turbulent flame area created by interactions between the flame and the eddies of the turbulent flow. If one considers the stabilization of a turbulent planar (on the average) flame, wherein the flame is statistically stationary with re-

* Corresponding author.
E-mail address: smmohan2@illinois.edu (S. Mohan).

https://doi.org/10.1016/j.combustflame.2021.111816
0010-2180/

spect to the incident isotropic turbulent velocity field, S_T would simply be the mean longitudinal incoming velocity. It is reasonable to expect Damköhler's hypothesis to be valid for other configurations; more relevantly in the current context to an expanding flame initiated from a small ignition source. Unlike a planar flame, outwardly growing flames are not statistically stationary and thus, no natural definition for a cross-sectional area A exists. Moreover, the flame segments constituting the flame surface propagate at different rates with the local flame speed conditioned on the local curvature of the surface and the underlying hydrodynamic strain rate. The variations in flame speed along the flame surface modify the turbulent flame speed relation (1), as previously discussed in [31]. Additionally, the determination of A_T is not solely due to turbulence; deformation of the flame surface may also arise from intrinsic flame instabilities which are themselves known to distort the flame even under laminar conditions.

The impact of the Darrieus-Landau (DL) instability on turbulent flames, which is known to distort the flames above a critical size in mixtures with an effective Lewis number greater than one [32,33], was noted in some early experiments [34,35] but its importance was generally deemed secondary to turbulence and thus largely overlooked. The interplay between the two competing effects was addressed systematically for nominally planar turbulent flames [31,36], and recent experiments [37–39] begun to examine its effect on outwardly expanding turbulent flames. Computational studies on this matter are still relatively sparse and their scope is often limited even for two dimensional flows, simply due to the sheer numerical cost associated with resolving the disparity in spatio-temporal scales. Additionally, most direct numerical simulations (DNS) are carried out in periodic domains which are at risk of simulating unrealistic flame turbulence interactions. Jenkins & Cant [40] performed a series of three dimensional DNS studies for unity Lewis number flames with single-step chemistry in periodic boxes to qualify the role of varying turbulence intensity levels on flame kernel wrinkling. They noted that the distribution in flame curvature broadened with increasing turbulence intensity. The effect of turbulence on the minimum kernel radius necessary to sustain combustion was investigated under a similar setup [41]. It was observed that in small kernels, the likelihood of extinction was greater due to imbalances in the heat generated from combustion and heat transfer from the kernel which was enhanced by turbulent transport. Thévenin et. al. [42] investigated the development of spherical premixed methane-air flames in a periodic box where they found that the mean flame radius increased considerably slower in 3D in comparison to 2D. However, these studies do not examine the long-time evolution of the flame kernel and are therefore unable to comment on the turbulent burning velocity. More recently, Fru et al. [43] examined the effect of varying turbulence intensity and equivalence ratio on the burning rate of methane-air flames in periodic domains where they saw that the consumption speed increased linearly with intensity before plateauing; a phenomenon known as the "bending-effect" first observed in experiments on expanding spherical flames [35,44].

Admittedly, whilst DNS remains the most comprehensive approach for studying turbulent combustion, the need for preserving a high enough spatio-temporal resolution to resolve flame-turbulence interactions and for adequately large domains to inhibit boundary effects from contaminating the solution, renders the problem cost-prohibitive. In addition, it becomes impractical when examination of large parametric spaces is needed, as is often necessary. More accessible approaches with modest computational requirements, such as Reynolds Averaged Navier-Stokes (RANS) or Large Eddy Simulation (LES), rely on closure assumptions and sub-grid models, making the validity and accuracy of their results difficult to assess. For example, the principle underlying assumption in RANS-type simulations pertinent to the current study is that the flame will preserve circular/spherical symmetry and variations in the thermochemical state of the mixture will solely be in the direction of flame propagation, i.e., the radial direction. Profiles of the flame front will not exhibit instantaneous distortions created by straining flow fields, such as pinching, pockets formation and subsequent consumption. These dynamics are known to enhance the burning rate and are affected greatly by the mixture properties. While temporal variations in spatially-averaged profiles such as flame brush thickness may be computed, solutions are limited in their ability to predict instabilities (hydrodynamic, thermo-diffusive) and other nonlinear phenomena such as cell formation/annihilation which are ubiquitous in large scale expanding flames and result in further enhancements in the overall burning rate. Effectively, such simulations assume *a priori* that any variation in the burning rate is purely turbulence driven.

The present work is based on a hydrodynamic theory [45–47] derived from general conservation laws using a rigorous asymptotic framework that leverages the various length scales associated with the combustion problem. The flame is treated as a boundary layer whose thickness is the smallest length-scale in the problem, i.e., the turbulence does not penetrate the flame zone and does not modify its internal structure. The flow on either side of the flame surface is described by the Navier-Stokes equations, supplemented by Rankine-Hugoniot jump relations that ensure mass, momentum and energy conservation across the flame. The flame propagation relative to the flow depends on the local stretch rate [48] (comprising of surface geometry and hydrodynamic strain-rate) modulated by a mixture-sensitive parameter, the Markstein length, which mimics the effects of diffusion and chemical reactions occurring inside the flame zone. The resulting nonlinear free boundary problem is characterized by two parameters namely the unburned-to-burned density ratio, or thermal expansion parameter, and the Markstein number. Varying them allows one to span a large parametric space of different fuel/oxidizer mixture types and pressure levels. Our methodology differs from the "G-equation" based approach in few aspects. The fully coupled nature of the hydrodynamic model accounts for both, flow acceleration resulting from gas expansion, and feedback of the local straining field and of geometrical variations in flame shape on the propagation, and the proposed numerical implementation readily admits multiply folded flame-surface solutions without requiring special treatment. Although the G-equation used for tracking the flame is similar, studies [49,50] using this approach have typically utilized precomputed velocity fields, thus unaffected by gas expansion, have restricted the flame to single-valued functions incapable of predicting folding and detachment, or have discounted the effects of straining or stretch completely, i.e., assuming the flame propagates either at a constant or curvature-dependent speed. Excluding the effect of hydrodynamic strain-rate is known to have a greater effect on the overall turbulent flame speed than curvature alone [31]. While studies within RANS and LES context, i.e., averaging or filtering the G-equation with closure assumptions for the correlation terms or for sub-grid variance of the G-function, accounted for the missing effects [51–54], the scalar-strain covariance contribution known to be dominant at scales on the order of the Markstein length were neglected.

The hydrodynamic theory performs exceptionally well for high-pressure deflagrations as the flame becomes increasingly thin. This aspect is of significant practical interest and a hurdle for other numerical approaches. Since the complexity of the chemistry is captured elegantly in a single physicochemical parameter, the restriction on both the numerical time-step as well as mesh size is alleviated making it ideal to study the turbulent expanding flames in physically meaningful domains. A further advantage of the current approach is the unambiguity associated with identifying the flame surface. Numerical and experimental studies often rely on a

specific temperature or species mass fraction iso-contour to identify the flame surface. Since such a choice is arbitrary, profiles of flame stretch and Markstein length estimated on this basis show great variability [55]. The proposed approach naturally lends itself to predict flame surface density profiles and flame brush thicknesses, both of which are comprehensive properties that can be used when comparing to experimental data, in addition to the burning velocity and/or velocity profiles.

Numerical implementations of the hydrodynamic theory have been previously used to investigate complex flame-turbulence interactions in two-dimensional [31,36,56,57] and three-dimensional [58] flows, using a planar configuration. The effect of systematically varying the turbulence intensity and integral length scale was compiled for a range of Markstein numbers representing mixtures of various composition, and used to isolate the influences of the DL instability from the turbulence. Despite the limitation on the lack of the effect of turbulence on the internal flame structure, the results were deduced from physical first principles, without invoking any turbulent combustion modeling assumptions or ad-hoc adjustable parameters. In this paper we examine the outwardly propagation of centrally ignited premixed flames. To simulate the propagation of the highly corrugated flame front on a Cartesian grid in an unconfined domain, the numerical methodology has undergone a major revision. The main modifications include improvements to the calculation of flame surface properties, such as curvature and stretch, without which inaccuracies will compound in time leading to erroneous predictions of the onset of instability and the overall burning rate. The aim is to assess the role of turbulence and its interplay with the DL instability during both, the early flame kernel development as well as its long-time evolution. Well-defined markers that point to the presence of the instability were identified to allow the quantification of DL influences on flame morphology and propagation speed and determine the extent to which such effects are enhanced/suppressed as turbulence characteristics quantified by turbulence intensity and integral length scale are varied. Among the novelties of the present results is the explicit dependency of the turbulent flame speed on physically-measurable quantities, and the manifestation of the DL instability on the scaling of the turbulent flame speed with turbulence intensity. Often, scaling law based on the square root of a modified Reynolds number were reported [23,24], but such expressions do not exhibit an explicit functional dependence on mixture properties, pressure, and even turbulence intensity. It should be noted that most experimental studies were confined to relatively small vessels with sizes ranging from 58 mm to 406 mm, but generally falling between 200 and 300 mm. Within this range, the turbulent burning velocity continually increases in time as the flame expands and become warped by the imposed turbulence, suggesting that the vessel may not be large enough for the turbulent burning velocity to converge to a steady value. Moreover, such experiments do not necessarily emulate freely-expanding flames as they are invariably associated with pressure buildup, temperature rise from adiabatic compression and possible acceleration effects. Experimental results also indicate that, due to its highly transient nature, the wrinkling of an outwardly expanding flame has a "memory" of the conditions upstream such that scaling laws for S_T must also depend on a turbulent time-scale which sets it apart from the "ideal" planar flame configuration cited earlier. And indeed, our results show that the turbulent flame speed exhibits a dependence on the mean flame radius, defined as a measure of the volume of fresh mixture consumed during combustion. In addition, we extract from the simulation data statistical properties of flame topology, in the form of probability density function (PDF) distributions of flame surface curvature and strain rate and their impact on the burning velocity.

2. Formulation

A premixed flame originating from an ignition point source, freely propagating into an infinitely large field of highly-vortical "turbulent" combustible mixture is considered. The hydrodynamic model described in the introduction is based on the assumption that the diffusion length that characterizes the flame thickness, $l_f = \mathcal{D}_{th}/S_L$ where $\mathcal{D}_{th}$ is the thermal diffusivity of the mixture, is much smaller than the characteristic length L of the hydrodynamic field corresponding, for example, to the average size of the corrugations formed on the flame surface. The evolution is followed once the flame attains a radius R_0, on the order of L, sufficiently larger than the flame thickness. In the limit, $\delta \equiv l_f/L \to 0$, the flame may be treated as a moving interface that separates the fresh mixture from the burned combustion products. It is expressed mathematically as the zeroth level set of a function $\psi(\mathbf{x}, t)$. The flow field $\mathbf{v}(\mathbf{x}, t)$ is obtained by integrating the Navier-Stokes equations, albeit with a small viscosity coefficient to allow for some dissipation, and imposing Rankine-Hugoniot conditions across the flame surface. The flow is affected by the gas expansion that results from the sharp change in density caused by the heat released due to combustion. The flame itself propagates relative to the flow ahead at a speed

$$S_f = S_L - \mathcal{L}\,\mathbb{K}\,, \tag{2}$$

interpreted as the laminar flame speed adjusted by the local stretch rate $\mathbb{K}$. The stretch rate consists of the combined effects of curvature and hydrodynamic strain-rate and is modulated by a Markstein length $\mathcal{L}$ which replicates the diffusive and chemical processes occurring inside the flame zone. Attention is restricted in this study to positive $\mathcal{L}$ corresponding to mixtures deficient in the more heavy component, such as lean hydrocarbon-air or rich hydrogen-air. Details of mathematical formulation, and the embedded-manifold/Navier-Stokes numerical methodology used to simulate the outwardly expanding flames are described in [59].

2.1. Turbulence generation

An algorithm based on the synthesis of divergence-free vector fields from a sample of Fourier harmonics is used to generate a homogeneous, isotropic flow field with specified characteristics (integral length scale ℓ and intensity u_0) that follows a model turbulence spectrum. Following [60–62] and adapted to a two-dimensional field, a spatial stochastic turbulent velocity is generated as a finite sum of N statistically independent random Fourier modes, namely

$$\mathbf{u}(\mathbf{x}) = 2\sum_{n=1}^{N} \tilde{u}_n \cos(\mathbf{k_n}\cdot\mathbf{x} + \varphi_n)\,\boldsymbol{\lambda}_n\,, \tag{3}$$

where $\boldsymbol{\lambda}_n = (\lambda_{x,n}, \lambda_{y,n})$ is the direction of the nth mode, whose amplitude and phase are given respectively by $\tilde{u}_n$ and φ_n. The wave vector $\mathbf{k}_n = (k_{n,x},\ k_{n,y})$ is selected randomly on a circle of radius $k_n = |\mathbf{k}_n|$ to ensure isotropy. This is accomplished by picking a random angle θ from a uniform distribution with probability density function, $p(\theta) = 1/2\pi$. The components of the wave vector are then $k_{n,x} = k_n\cos\theta$ and $k_{n,y} = k_n\sin\theta$. The phase φ_n is chosen from a uniform probability distribution to obtain a homogeneous field and, for isotropy, the probability density function $p(\varphi_n) = 1/\pi$ with $-\pi/2 \le \varphi \le \pi/2$.

The imposition of the incompressibility constraint on the turbulent field involves satisfying $\mathbf{k_n}\cdot\boldsymbol{\lambda}_n = 0$ for each mode n which arises as a solution to the following condition,

$$\nabla\cdot\mathbf{u} = -2\sum_{n=1}^{N} \tilde{u}_n\,(\mathbf{k_n}\cdot\boldsymbol{\lambda}_n)\,\sin(\mathbf{k_n}\cdot\mathbf{x} + \varphi_n) = 0.$$

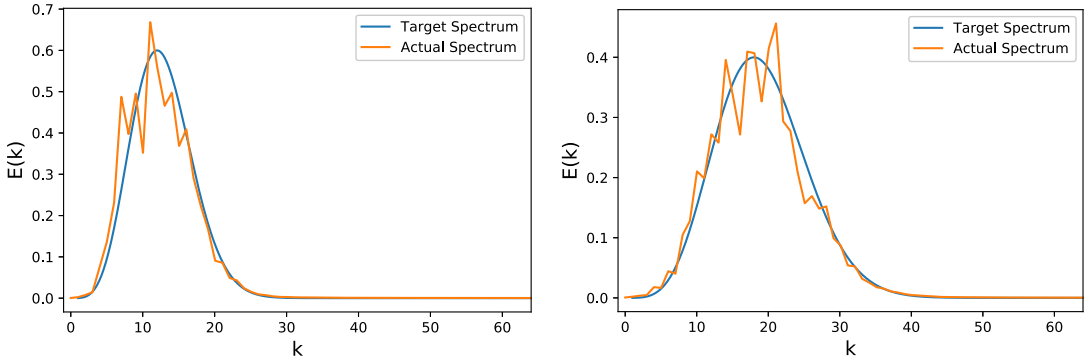

(a) $k_0 = 12$ (b) $k_0 = 18$

Fig. 1. Comparison between the target (input) spectrum and the actual computed two-dimensional spectrum at different integral length scales $\sim k_0^{-1}$.

The amplitude $\tilde{u}_n$ of each mode is determined from the turbulent kinetic energy spectrum $E(k)$. Since the N modes are statistically independent, the turbulent kinetic energy $\bar{k}$ is given by

$$\bar{k} = \sum_{n=1}^{N} \tilde{u}_n^2$$

such that $\tilde{u}_n = \sqrt{E(k_n)\,\Delta k_n}$. As suggested in [62], a logarithmic distribution of the N modes provide a better discretization of the spectrum E in the lower wavenumber range, which corresponds to the larger energy containing eddies. Accordingly,

$$k_n = \exp\left[\ln k_1 + (n-1)dk_l\right], \qquad n = 1, ..., N$$

where $dk_l = (k_N - k_1)/(N-1)$. Here $k_1 = 2\pi/L$ represents the smallest wavenumber (scaled with domain width L), whereas $k_N = \pi/dx$ is the largest wavenumber that can be represented on the Cartesian grid (restricted by the Nyquist frequency). The spectrum taken from Kraichnan [60] and adapted for a two dimensional turbulent field is given by

$$E(k) = \frac{2}{3}\left[16\sqrt{\frac{2}{\pi}}u_0^2\frac{k^4}{k_0^5}\exp\left(-2\frac{k^2}{k_0^2}\right)\right]$$

such that

$$\int_0^\infty E(k)dk = u_0^2$$

where u_0 is the root-mean-square (r.m.s) velocity, and the energy spectrum peaks at $k = k_0$ which indirectly modulates the size of the integral scale. Since the generated turbulence is assumed to be homogeneous and isotropic, the integral length scale l is obtained from,

$$l = \frac{\int_0^\infty k^{-1}E(k)dk}{\int_0^\infty E(k)dk}.$$

The effect of varying the integral scale is examined in terms of how well the targeted energy spectrum is attained. Shown in Fig. 1 is a comparison of the computed energy spectrum, determined on a square domain of width 2π to the targeted spectrum (with no boundary conditions imposed), for r.m.s velocity $u_0 = 2.5$ and two values of k_0. Representative turbulent fields are shown in Fig. 2, where the visualization is depicted by means of vorticity iso-contours. These fields were obtained after the initial velocity created from (3) has evolved nearly twenty iterations using the Navier-Stokes equations, and was verified to satisfy the incompressibility conditions to within four decimals.

2.2. Flame propagation

A pre-generated homogeneous isotropic turbulent flow field with zero mean, similar to the one shown in Fig. 2, is introduced into a large square domain. This initial velocity field is characterized by two control parameters; the turbulence intensity u_0 (the r.m.s of velocity fluctuations), scaled with respect to S_L, and the wavenumber k_0 at which the energy spectrum peaks that modulates the integral length scale ℓ scaled with respect to R_0.

A laminar flame kernel of radius R_0 is then initialized at the centre of the computational domain and followed in time. A domain of size $96R_0$ was deemed large enough through numerical experimentation to ensure that boundary effects do not pollute the growing flame solution. Realistic zero-Neumann boundary conditions are prescribed for ψ and $\mathbf{v}$ in the far field. The pressure is set equal to zero hence simulating an open, constant pressure domain. Since the turbulent kinetic energy decays in time, the stopping criteria used for simulations was determined by computing the time taken for approximately a 20% decrease in the turbulent kinetic energy of the computational domain in the absence of combustion, for each value of u_0. The integral length scale is meanwhile known to grow due to the inverse energy cascade that characterizes two dimensional turbulence.

The intensity u_0 represents the turnover velocity of the energy carrying eddies of size ℓ. Within the current context, the relevant length scales are only those larger than the Gibson scale $\ell_G \sim \ell u_0^{-3}$, as discussed by Peters [63]. Effectively, this implies that the flame behaves as a band pass filter and that eddies larger than ℓ_G are able to wrinkle and fold the flame surface, whilst all remaining eddies, down to the Kolmogorov length scales, are not energetic enough to interact with and affect the flame. Therefore, all flame-turbulence interactions are purely advective and kinematic in nature and scales smaller than ℓ_G need not be resolved. To this end, all reported simulations are performed with a grid resolution of 128 points per unit length R_0, equating to an overall domain with $(128 \text{ x } 96)^2 = 12288^2$, or nearly 150 million grid cells.

3. Results

Figure 3 shows a highly corrugated flame that resulted from interaction with a vortical flow of initial intensity $u_0 = 5.0$, after expanding to approximately 15 times its initial radius. The flame surface, defined unambiguously as the zeroth level set of the function $\psi(\mathbf{x}, t)$, is represented by the black solid curve(s) and the turbulent flow is visualized by counter-rotating vortices (blue/red). The flow in the burned gas region remains turbulent, but with significantly reduced intensity due to gas expansion. The figure illus-

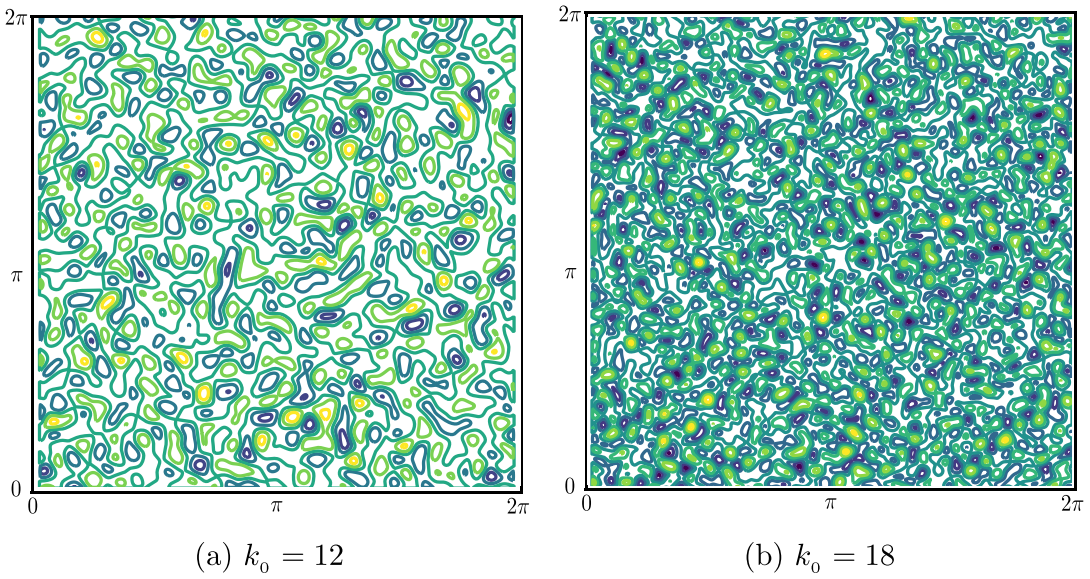

Fig. 2. Representative turbulent flow fields used as initial states for the outgrowing flame studies, for r.m.s velocity $u_0 = 2.5$ and two values of k_0; the flow field is visualised by means of vorticity iso-contours.

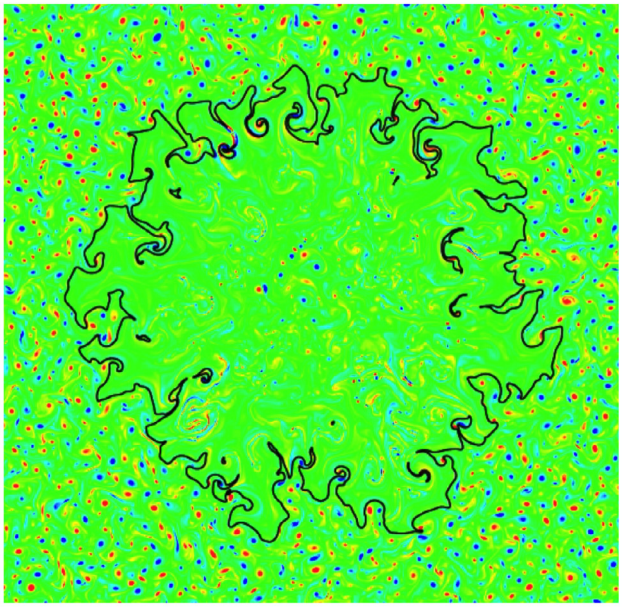

Fig. 3. Outwardly propagating flame in a turbulent media of initial intensity $u_0 = 5.0$, after reaching approximately 15 times its initial radius. The flame surface is represented by the black solid curve and the turbulent flow is visualized by the blue/red counter-rotating vortices.

trates the merits of the hydrodynamic model; it enables tracking multiply-folded surfaces arising from flame pinch-off and pocket formation, all of which have been observed in laboratory experiments. These characteristics enable a thorough investigation of various flame properties, including flame shape and its fractal dimension, flame surface density, flame brush thickness and turbulent flame speed, and their dependence on the thermal expansion parameter σ, controlled by the heat release, and the reduced Markstein number $\mathcal{M} = \mathcal{L}/R_0$, representing the mixture composition. The Markstein number $\mathcal{M}$ differs from conventional definition, which is scaled with respect to the flame thickness l_f, by a factor l_f/R_0.

In the results reported below, $\sigma = 6$ is adopted for all simulations, with $0.02 \leq \mathcal{M} \leq 0.04$ to accommodate a wide range of conditions as reported in [31]. Table 2 of the referenced paper provides values of the calculated Markstein length $\mathcal{L}$ for propane-air and hydrogen-air mixtures over a range of equivalence ratios dictated by the values of l_f, with $\delta \sim 0.01$. Since typically $L \sim R_0/5$, as suggested from linear stability theory, the simulations correspond to $R_0 \sim 5$ - 25 mm. The scope is limited to discussing mixtures which admit positive Markstein lengths to prevent the flame from being contaminated by thermo-diffusive instabilities. The values were chosen to accommodate conditions where the onset of the DL instability develops at different stages of the propagation. Linear stability results [59] show that the instability is significantly delayed for $\mathcal{M} = 0.04$ in comparison to $\mathcal{M} = 0.02$, thus allowing for sub- and super-critical flame behaviors, appropriating the nomenclature used for planar flames [31]. The initial turbulence intensity was varied from $0.1 \leq u_0 \leq 5.0$, with the energy spectrum peaking at two select wavenumbers, namely $k_0 = 12$ and $k_0 = 18$ corresponding to $\ell \approx 0.086$ and $\ell \approx 0.056$, respectively. The dependence of flame characteristics on the integral scale ℓ and thermal expansion parameter σ will be examined in future studies.

Figure 4 depicts the flame evolution for $\mathcal{M}=0.02$ at approximately equal spatial intervals. The flame is evolving into a turbulent field of initial intensity $u_0=1.0$ and integral length scale $\ell \approx 0.086$. The flame, which has expanded more than 20 times its initial radius, is seen to retain a mean circular shape. Shortly after initiation, the flame acquires a cellular structure with deep grooves protruding into the burned gas. The persistence of these cusp-like structures during the entire propagation indicates that the DL instability is playing an active role by enhancing the flame surface area in addition to enhancements arising through flame-turbulence interactions. In a laminar setting, these conformations have been shown to contribute to a substantial increase in the overall propagation speed relative to the laminar flame speed. Another attribute of the nonlinear effects beyond the instability threshold is the annihilation events, wherein flame's area is destroyed when two cusps merge into a single cusp-like structure [64]. The impact of the vortical flow is evident in that even at this moderate turbulence intensity the flame folds in unto itself, becoming multivalued in the polar direction.

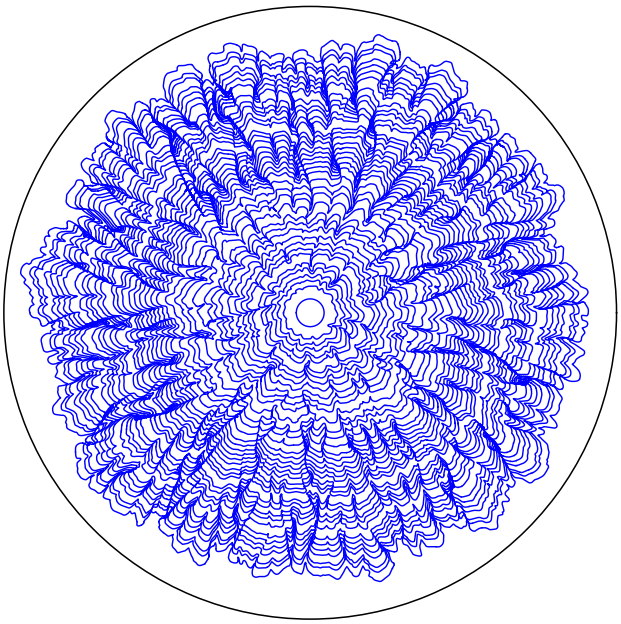

Fig. 4. Ensemble of instantaneous flame shapes at equal spatial intervals; the flame is expanding into a turbulent field of initial intensity $u_0 = 1.0$ and integral scale $\ell \approx 0.086$, and the mixture corresponds to $\mathcal{M} = 0.02$ and $\sigma = 6.0$. The larger (black) circle corresponds to approximately 60% of the domain of integration.

3.1. Effects of turbulence intensity and scale

Figure 5 illustrates the flame evolution for various initial turbulence intensities (the case for $u_0 = 1.0$ is shown in Fig. 4). For low intensities, $u_0 = 0.10$ and 0.25, the flames visually appear laminar and similar to the evolution observed in a quiescent mixture at the onset of the DL instability and during the following nonlinear development [59,65]. It can be seen that while cell splitting is pervasive in both cases, the characteristic size of the structures are considerably smaller for the larger intensity $u_0 = 0.25$, in relation to the same overall flame radius, owing to increased likelihood of cell splitting. Predictably, the amplitude of the disturbances are notably larger with larger initial upstream disturbances. Flame perturbations induced by the flow field are overwhelmed by the spontaneous growth of cusp-like structures, cell splitting and amalgamation that dominate the flame surface development. The flame appears resilient to the turbulence, a feature previously observed in planar flames at similar conditions [36,58]. At these low intensities, the flame retains a memory of the initial cracks as they appear on the flame surface. This behavior was initially reported in DNS studies of outwardly propagating lean premixed hydrogen-air flames in laminar flows [66]. It was observed that the form of the initial perturbation dictates the wavelengths of the DL cells that develop on the surface. The initial form of the perturbation (monochromatic or polychromatic) determines the maximum wavelength of the cells that would populate the surface and eventually, when the cells themselves become large enough, secondary cells which are integer factors of the primary wavelength become prominent while the position of the primary crack is retained and dictates the long-term evolution of the flame front shape. A similar representation is seen in Figs. 5a and 5b where the eddies of different sizes behave as continuous polychromatic perturbations on the front. At elevated initial turbulence intensities, these disturbances form irregular structures that are more evenly distributed throughout the flame surface as opposed to the large straight cracks that appear under quiescent conditions and low-to-moderate turbulence intensity levels. The presence of the DL cusps are less discernible and the proclivity for pocket formation is increased. When all the experiments are compared at the same mean radius, it can be clearly seen that the distribution of cell sizes is far greater as u_0 is increased, and smaller cell sizes are observed in addition to the higher amplitude disturbances. Three regimes can thus be identified: (i) the instability dominated regime, (ii) the instability-turbulence interaction regime and (iii) the turbulence dominated regime. Flame folding, pinch-off and pocket formation observed in Fig. 3 are a hallmark of the latter.

An examination of the change in total *flame area*, i.e., the area enclosed by the zeroth level set which effectively measures the volume (area in 2-D) of burned gas, scaled with respect to the square of the mean flame radius (defined precisely later) is performed. Each subfigure in Fig. 6 shows the flame area as a function of time under different turbulent flow conditions. Two distinct values of the Markstein number are considered, $\mathcal{M} = 0.02$ and $\mathcal{M} = 0.03$, with the smaller value representing a mixture for which the manifestation of the DL instability is expected to be observed at an earlier time. With increasing u_0, an enhanced interaction between the flame and turbulent eddies is observed. This results in a much more intense wrinkling of the flame surface and in turn, a rapid increase in total flame area. DNS studies of spherically expanding flames under laminar [67] and turbulent [68] conditions have shown that the global burning rate, namely the integral of the heat release rate over the whole domain, is directly proportional to the flame area, indicating that the mechanism responsible for the increase in the global burning rate at higher intensities is the stronger wrinkling of the flame surface due to its interaction with more energetic vortices. This general behavior is observed for all the mixtures that were investigated albeit to varying degrees, suggesting that flame area increase is relatively the more dominant cause for the increase in propagation speed than local effects, such as flame stretch which are tempered by mixture properties.

3.2. Flame surface area

It is reasonable to expect that with appropriate modifications, Damköhler's turbulent flame speed relation (1), conjectured for a planar configuration, could be applied for expanding circular/spherical flames. The initial focus is on the evaluation of the area ratio A_T/A. The surface area of a turbulent flame A_T can be obtained by summing the lengths of all the adjoining segments of a corrugated flame in 2-D, or the patches of all surface elements of the corrugated flame in 3-D. This includes the area created during pinch off and subsequent destruction when pockets of unburned gas are consumed. The issue lies in constructing an appropriate definition of the cross-sectional area A which, for the present case is not an obvious choice, considering that outwardly growing flames are not statistically stationary. One option is to express A as the surface area (flame length in 2-D) of a unperturbed spherical (circular) flame kernel whose radius is equal to the mean radius of the turbulent flame [68]. This method of measuring A, i.e., by directly processing instantaneous flame shapes, is widely accepted in experimental studies [22,69]. A more suitable choice[1] is to determine A as the surface area of the unperturbed spherical (circular in 2-D) flame kernel that encompasses the same volume of burned gas (area in 2-D) confined by the corrugated turbulent flame. If $\mathbb{V}_b$ is the total volume (area in 2-D) of burned gas computed from the simulations at time t, the mean radius for a spherical (circular) flame is defined from

$$\langle R \rangle_{3D} = \left(3\mathbb{V}_b/4\pi\right)^{1/3}, \qquad \langle R \rangle_{2D} = \sqrt{\mathbb{V}_b/\pi}$$

[1] A choice that leads to physically more consistent results for the dependence of S_T on the mean flame radius, as shown in Figs. 7–11.

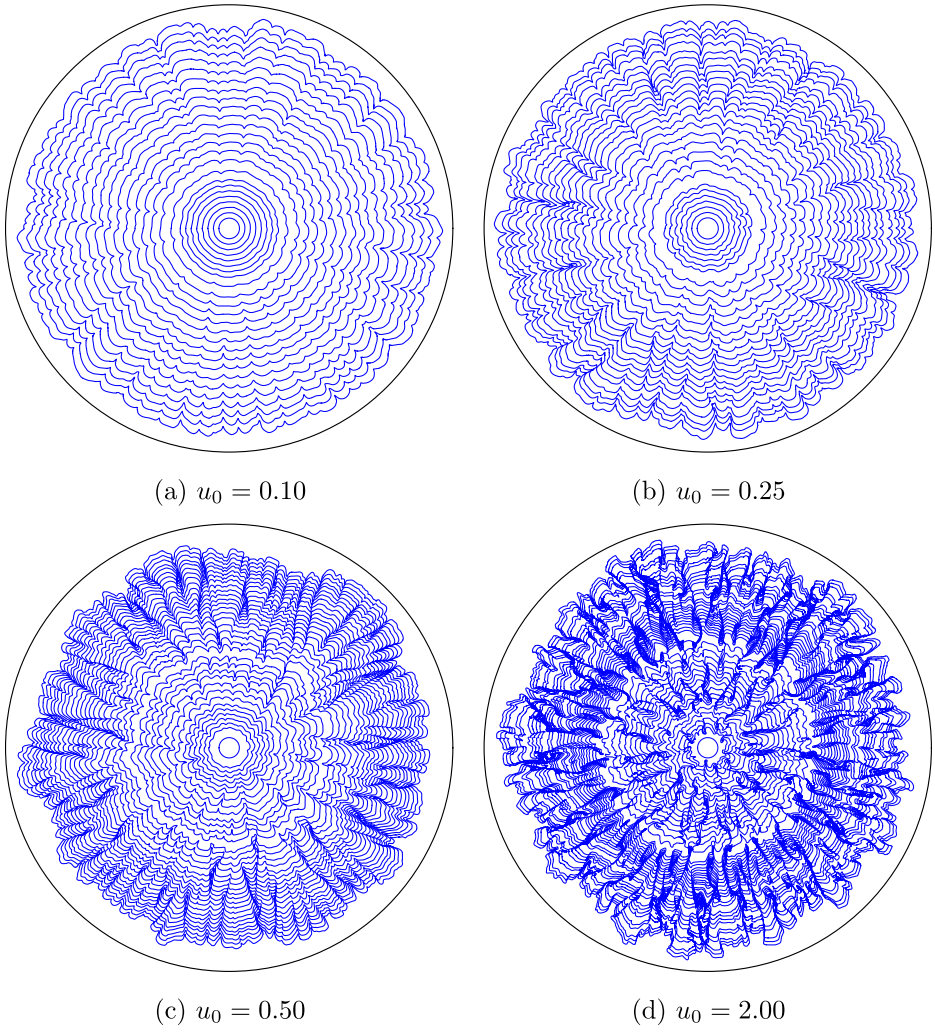

Fig. 5. Flame surface evolution (at equal spatial intervals) for varying initial turbulence intensities and integral scale $\ell \approx 0.086$; corresponding to $\sigma = 6.0$, $\mathcal{M} = 0.02$. The larger (black) circles correspond to approximately 60% of the domain of integration.

and the cross-sectional area is $A = 4\pi \langle R \rangle^2$ for a spherical and $A = 2\pi \langle R \rangle$ for a circular flame. Hence, by normalizing the total surface area of the flame with A, the effect of turbulence on flame wrinkling around a mean radius can be isolated. It should be emphasized that the volume of burned gas at large values of u_0 is significantly larger than at low values of u_0 due to the high degree of wrinkling, as seen in Fig. 5. Consequently, the mean position $\langle R \rangle$ does not be necessarily correspond to the instantaneous position of the flame relative to the initial kernel.

This renormalization of A_T is graphed in Fig. 7, which shows the variations in A_T/A as a function of the mean flame radius $\langle R \rangle$ for different turbulence and mixture conditions. Based on Damköhler's expression (1) it would also correspond to the turbulent flame speed S_T, scaled with respect to S_L. Since the flame is intrinsically unsteady, the area ratio, or S_T in this context, depends on the mean flame radius, and therefore on the turbulent time-scale. Initially, the speed increases at a rate that depends on the turbulent and flow conditions, but at long times the growth rate diminishes and the turbulent flame speed reaches a constant value which depends primarily on the turbulence intensity and scale, with only small changes resulting from variations in mixture conditions. The renormalization may be qualitatively interpreted as the amount of wrinkling per unit flame length (or area). This quantity should exhibit converging tendencies considering the nearly constant amount of turbulent vortical motion encountered by the flame front and also due to the minimum cutoff wavelength of disturbances that can be supported. The cell sizes for an expanding flame can neither be larger than the mean flame radius nor smaller than the flame thickness; more specifically, the unstable modes resulting from the DL instability [59] are limited to the range of wavelengths $\lambda_{\min} < \lambda < \lambda_{\max}$ where $\lambda_{\min} \sim l_f$ and $\lambda_{\max} \sim \langle R \rangle$.

The asymptotic tendencies shown above are better captured by analyzing the temporal variations in fractal dimension of the flame surface, a quantity that can be used to measure the extent of wrinkling of the flame surface. Figure 8 shows the variation of the fractal dimension d as a function of $\langle R \rangle$, using the methodology described in [64]. As the flame radius becomes large, there is a "saturation" of the wrinkling/fractal dimension such that relative to the expanding flame the rate of increase of the wrinkled flame surface area tends towards a constant. Consequently, the rate of increase in area ratio, which depends on the extent of wrinkling, tends towards an asymptotic constant value.

The relative role of the DL instability can be gleaned from this image. For lower turbulence intensities, the fractal dimension remains relatively unchanged initially before growing abruptly when the flame radius increases. Visually, this coincides with the emergence of cusps along the flame surface, indicating the onset of the instability. For larger intensities, this bifurcative behavior becomes

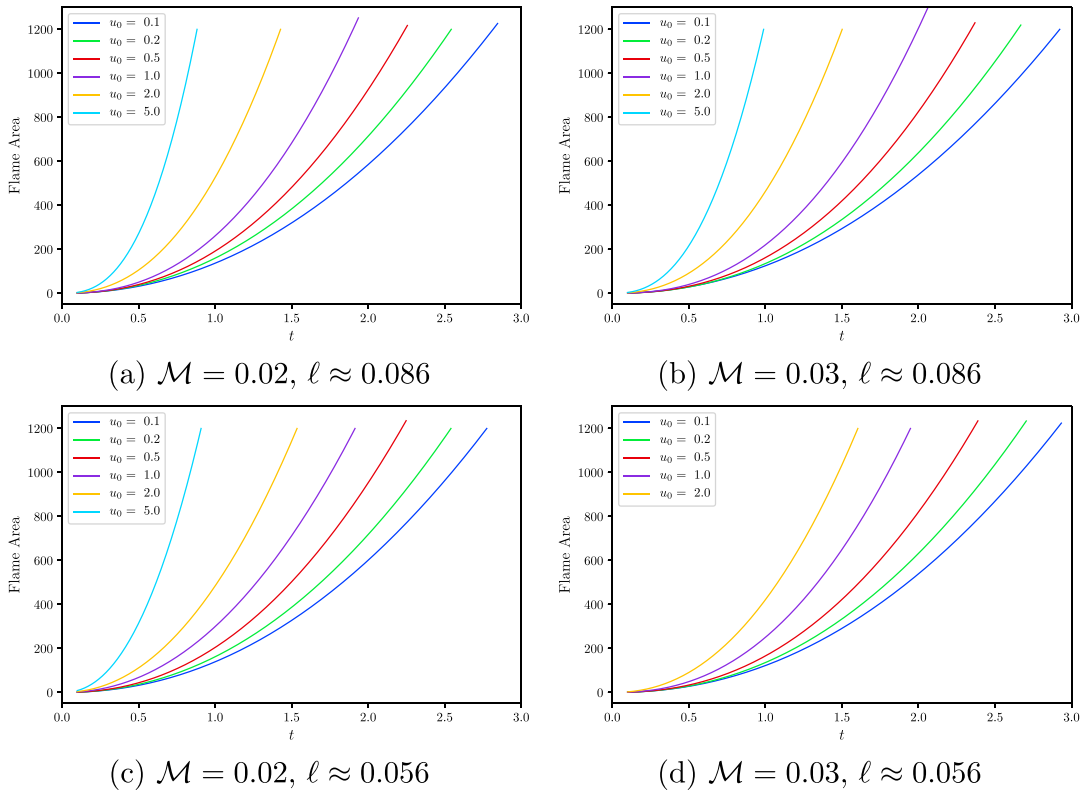

Fig. 6. Temporal evolution of the *flame area* - total area (volume in 3-D) of burned gas, during the simulation of expanding flames for different turbulence and mixture conditions.

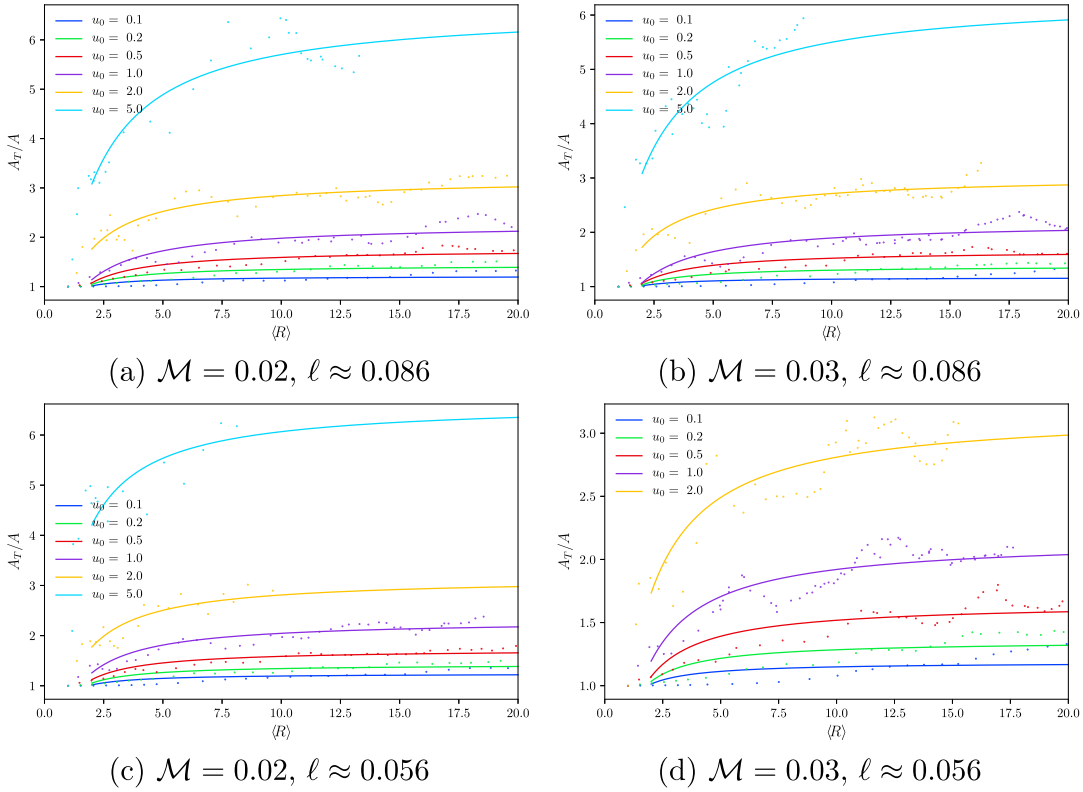

Fig. 7. Temporal variations of the scaled turbulent flame speed S_T/S_L, based on Damköhler's expression (1) , for different turbulence and mixture conditions. Note the different scale of the ordinate in (d).

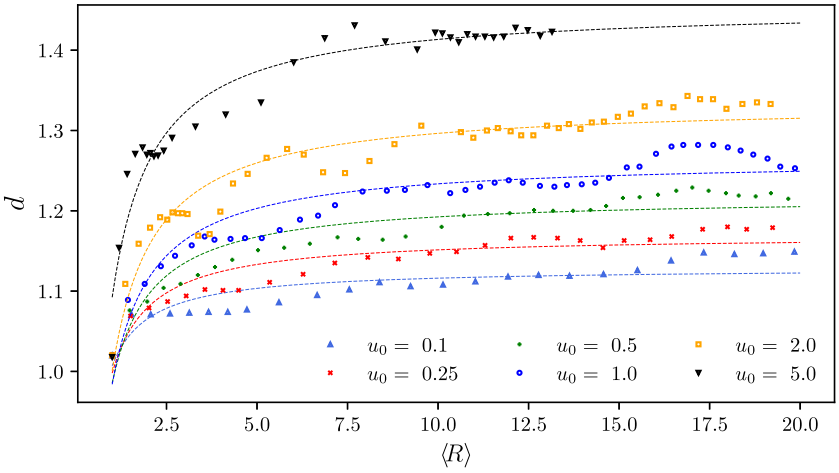

Fig. 8. Temporal variation in the fractal dimension of the flame surface for different initial turbulence intensities, for $\mathcal{M} = 0.02$ and an integral scale $\ell \approx 0.086$, showing that the fractal dimension and hence the extent of wrinkling plateaus out for large flame radii.

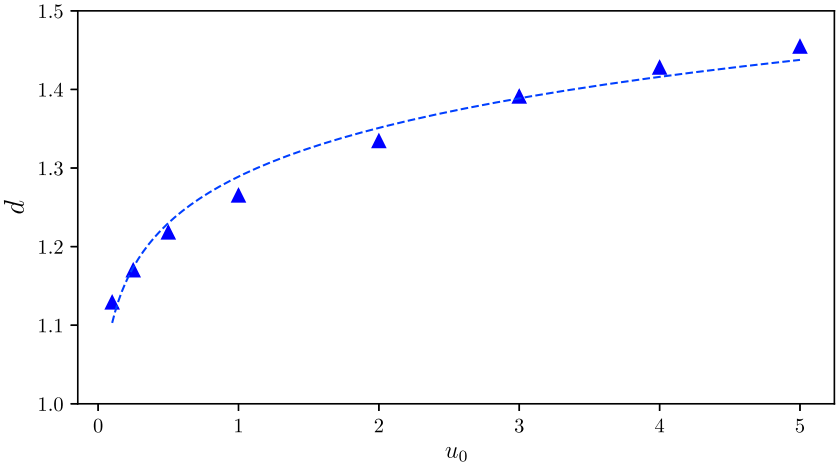

Fig. 9. The increase in fractal dimension, a measure of the amount of wrinkling on the flame surface, as a function of the turbulence intensity u_0 for $\mathcal{M} = 0.02$ and an integral scale $\ell = 0.086$, extracted from Fig. 8 once the flame has grown significantly large.

less distinct and eventually disappears altogether; the fractal dimension immediately begins to grow as turbulent eddies start to wrinkle the flame surface. This suggests that the stabilizing influences exerted by flame stretch become less effective when large upstream flow disturbances are present. The converged values of the fractal dimension for various intensities extracted from this graph is shown in Fig. 9.

3.3. Instability vs turbulence wrinkling

It is instructive to examine the growth rate of various perturbations at different turbulence intensities. At each instant, the (normalized) perturbations on the flame surface are obtained from the deviation of the local radius R from the mean value $\langle R \rangle$. A Discrete Fast Fourier Transform (DFFT) of the resulting signal is then taken to compute the amplitude of disturbances of wavenumber k and the *initial* growth rates of a select of wavenumbers are plotted in Fig. 10 for $u_0 = 0.1, 0.5$ and 1.0. The unreported values either do not exhibit a meaningful growth rate over the duration considered, or cannot be properly differentiated due to the highly nonlinear conformations present on the flame surface.

Consistent with the observations in Fig. 8, the growth rates for $u_0 = 0.1$ are initially small. The underlying flame expands faster than the perturbations induced by the upstream turbulence are able to grow, and the flame surface remains smooth as in its initial state. At $\langle R \rangle = 1.75$, the perturbation corresponding to a specific wavenumber, $k = 13$, starts to growth before all others. In this regime, given the delay in the onset of the instability, it is clear that the growth rate induced by the DL instability is greater than that induced by turbulence fluctuations for all wavenumbers in the turbulence spectrum. For $u_0 = 0.5$, the delay is greatly reduced, and disturbances corresponding to $k = 14$ and $k = 15$ begin growing almost instantaneously. The amplitude of the turbulence-induced fluctuations overwhelm the stabilizing influence of stretch resulting in a wrinkled flame from the outset of the propagation, which is reflected in the enhancement of the fractal dimension. Meanwhile, the growth rates corresponding to the lower wavenumbers $k = 9$, 13 remain suppressed initially, growing at timescales comparable to, or marginally larger than, the effectively unperturbed or weak turbulence intensity case discussed earlier. While it is not definitive whether the eventual growth is instability-driven or turbulence-induced, it can be speculated that the turbulence wrinkles the flame surface initially, resulting in locally larger stretch rates. The flame must therefore attain a larger radius before the stabilizing influences of stretch are diminished

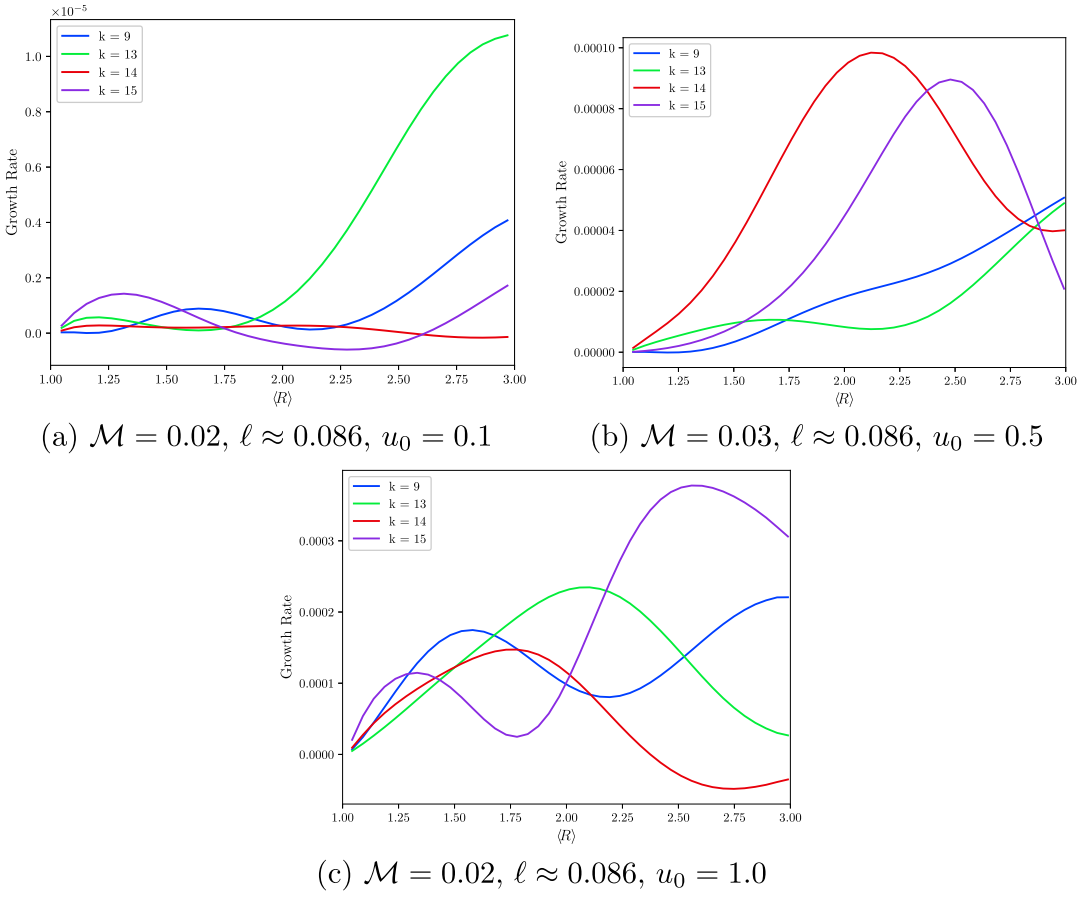

Fig. 10. Temporal variations of the initial normalized growth rate of disturbances with wavenumber k, extracted from the simulations.

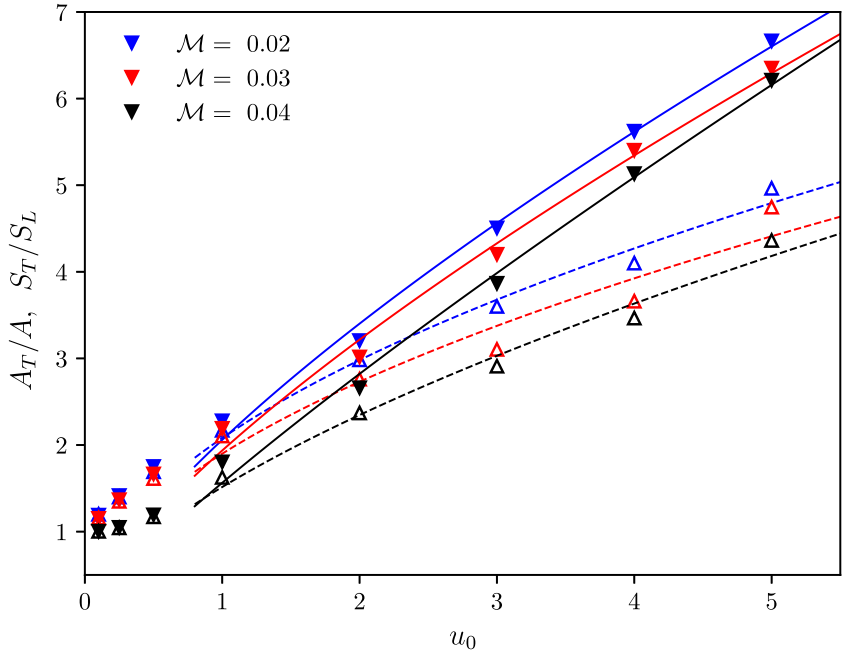

Fig. 11. The area ratio A_T/A (solid curves) and turbulent flame speed S_T/S_L (dashed curves) as a function the turbulence intensity u_0, for $\ell \approx 0.086$ and various values of the Markstein number.

Table 1
The coefficients of the scaling laws (5) for the area ratio and turbulent flame speed, corresponding to $\sigma = 6$.

$\mathcal{M}$	ℓ	b	n	c	m
0.02	0.086	2.05	0.72	2.08	0.52
	0.056	2.39	0.61	2.34	0.48
0.03	0.086	1.93	0.74	1.90	0.53
	0.056	2.32	0.66	2.28	0.40
0.04	0.086	1.56	0.85	1.51	0.63
	0.056	1.51	0.85	1.47	0.68

for the instability to start developing and potentially overwhelming the growth of turbulence-induced wrinkling. This blend of different factors contributing to the surface corrugations is commensurate with the wrinkling pattern observed on the flame surface in Fig. 5c. For $u_0 = 1.0$, all perturbations exhibit instantaneously strong positive growth rates, by an order of magnitude larger than those observed for $u_0 = 0.5$, which demonstrates the clear overwhelming nature of the turbulence.

The present work demonstrates that increases in turbulence intensity reduces the range of radii over which the flame remains impervious to perturbations. While this is in agreement with experimental observations [37], it does not support the hypothesis put forth that the critical radius for the DL instability is necessarily smaller under quiescent conditions than it is under turbulent conditions. In fact, the opposite trend is observed.

3.4. Turbulent flame speed

As noted in the introduction, the relation (1) for the turbulent flame speed proposed by Damköhler assumes that the local speed of the corrugated flame is constant along its surface and does not account for the reduction (for $\mathcal{L} > 0$) resulting from stretching effects, which are substantial especially at larger turbulence intensities. The modification of this expression, as discussed in [31], leads to

$$\frac{S_T}{S_L} = \overline{\frac{S_f}{S_L}\frac{A_T}{A}} \tag{4}$$

where A_T is, as before, the surface area of the turbulent flame and the mean (denoted by the "overline") is the average over the entire flame surface area. The implication is that the variation in overall burning rate due to the turbulence is affected by contributions other than simply the increase in flame surface area. The approximate long-time values of the area ratio A_T/A extracted from the data in Fig. 7, and of the corresponding stretch compensated modification, or turbulent flame speed S_T/S_L, are plotted as a function of the initial turbulence intensity in Fig. 11 for $\ell \approx 0.086$ and three different Markstein numbers. Similar curves result for the integral length $\ell \approx 0.056$. One observes that Damköhler's relation (1) overestimates the turbulent flame speed with the variance becoming more pronounced when increasing u_0; for $u_0 = 5$, for example, the discrepancy is nearly 25%.

For the moderate turbulence intensities considered in the present simulations, the area ratio and turbulent flame speed exhibit sub-linear dependence on the initial turbulence intensity u_0 of the form

$$\frac{A_T}{A} = b\,u_0^n \qquad \frac{S_T}{S_L} = c\,u_0^m, \tag{5}$$

with coefficients b, c and exponents n, m depending on the integral length scale ℓ, Markstein number $\mathcal{M}$ and thermal expansion parameter σ. Their values for the parameters examined in this study are listed in Table 1.

The coefficient b is inversely correlated with the Markstein number $\mathcal{M}$, a result of the decrease in local flame speed due to flame stretch and to the susceptibility of the flame to the DL instability. The difference in A_T/A gradually diminishes when the turbulence intensity increases indicating that the DL mechanism is progressively becoming overwhelmed by the turbulence, leading to a singular behavior emerging regardless of the mixture type or susceptibility to the instability. Experimental studies [34,35,37,39] of expanding spherical flames have also pointed to this narrow range of intensities in which the DL instability is dominant.

Meanwhile, the effect of a smaller integral length scale appears more pronounced at the larger $\mathcal{M}$ where the flame propagation is not dominated by the DL instability. In general, however, no systematic dependence was observed with varying integral length scale. The existence of a critical integral length scale that leads to maximum amplification in the turbulence burning velocity was postulated theoretically [70] and noted in studies within the hydrodynamic framework [57,71] for planar configurations. This critical integral scale was found to exhibit a weak dependence on the mixture's Markstein number under low-to-moderate intensity levels. It should be noted that the current simulations appear to be far removed from this critical integral length scale reported in [57] and may offer an explanation for the limited variability exhibited with changing integral length scale. Other studies corroborate strong correlation of S_T/S_L with respect to u_0 but comparatively weaker ones with ℓ; for example, $S_T/S_L \sim u_0^{3/4}\ell^{1/4}$ and $S_T/S_L \sim u_0^{1/2}\ell^{1/6}$ were proposed in [5,72]. Given the sparsity of data available in the current work, further work is required to assess the effect of varying integral length scale.

3.5. Turbulent flame brush

A meaningful definition of the turbulent flame speed is impeded by the fact that the speed of any iso-scalar contour representing the flame surface is affected not only by the conversion of reactants into products, or the local flame speed, but also by the growth of the mean thickness of the flame brush. This quantity measures, to some degree, the influence of the physico-chemical and turbulence parameters on the overall flame structure. Its determination is of great interest because it constitutes an intrinsic length scale in the flamelet regime of turbulent combustion, it has a universal normalizing property and it globally characterizes a turbulent premixed flame.

Figure 12 is an illustration of the flame brush for increasing values of initial turbulence intensities, used to draw parallels with turbulent planar flame studies. Each subfigure depicts an ensemble of flame surfaces at different instances, at times after the flame wrinkles have "saturated", clipped appropriately and superimposed over a fixed interval. Considering that the outwardly propagating flames are non-stationary and their angular extent is varying in time, the thickness of the flame brush may be determined from the deviation of the flame position R from its mean position $\langle R \rangle$ and normalised by the same radius in order to allow for a clean comparison across the various different intensities. The flame brush thickness is thus given by

$$\Delta R = \frac{R - \langle R \rangle}{\langle R \rangle}.$$

For low values of u_0, the width of the resulting flame brush is relatively narrow with $-0.05 < \Delta R < 0.05$. There are prominent sharp cusps tailing towards the burned gas that indicate the presence of the DL instability, which is the foremost contributor to the width of the flame brush. As the turbulence intensity is increased, there is a visible growth in ΔR; the amplitude of the cusps becomes far more pronounced and the brush appears far more distributed. At the moderate intensity of $u_0 = 1.0$, folds on the flame surface become evident and pockets of unburned gas are seen detaching

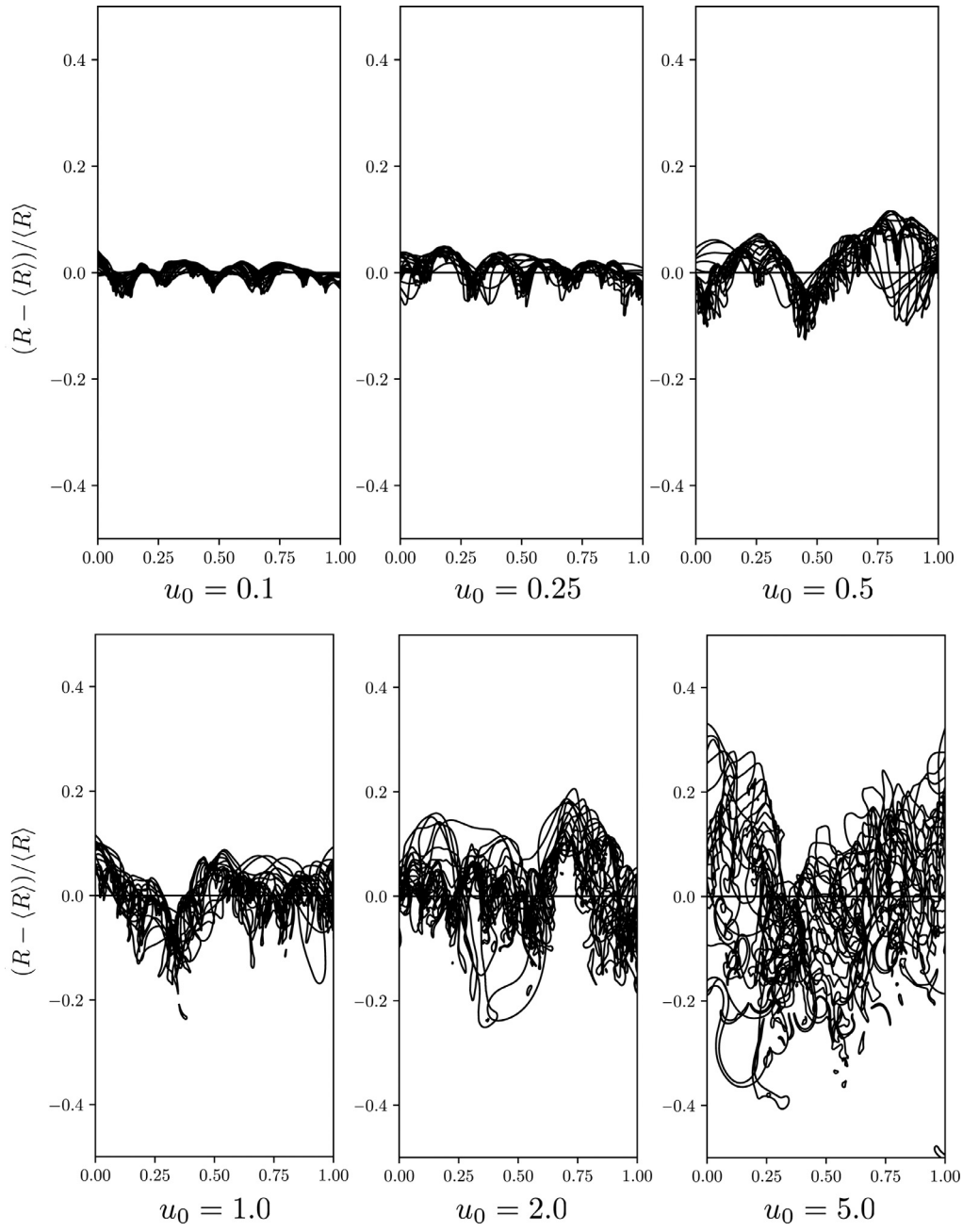

Fig. 12. Visualization of the flame brush for increasing values of the turbulence intensity u_0, extracted from simulations with $\ell \approx 0.086$ and $\mathcal{M} = 0.02$. The flame brush was created by superimposing realizations at large radii where the flame wrinkles have "saturated", as corroborated by the constant asymptotic fractal dimension, and the data was clipped for $0 < \theta < 1$ in order to present ΔR over a fixed interval.

from the flame surface. The number of negatively curved cusp-like flame segments start to diminish and the flame brush on the whole begins to appear more symmetric about $\Delta R = 0$. At higher intensities still, $u_0 = 5.0$, the flame brush is much thicker, more distributed and less concentrated about the mean. There are long tails of unburned pockets protruding into the burned gas with an increased propensity of pockets to form. There is also far less variation in the width of the flame brush along the transverse direction.

The discussion thus far has relied on a qualitative descriptions. For a quantitative definition of the flame brush thickness, a progress variable map C is computed by constructing a cumulative probability distribution of the flame position. It takes values from $C = 0$ on the unburned side to $C = 1$ on the burned side. The variations in the flame brush thickness δ_T can then be determined from the profiles of the mean progress variable $\langle C \rangle$ plotted against the mean flame position $\langle R \rangle$. The product $\langle C \rangle \big[1 - \langle C \rangle\big]$ can then be thought as the probability of encountering a flame front at some point within the flame brush region. While this approach does not capture variations of C in the azimuthal direction, only in the radial direction, it does account for pocket formation and consumption. A sample progress variable is shown in Fig. 13 for $\mathcal{M} = 0.02$, $\ell \approx 0.086$ and $u_0 = 1$ at different time intervals. As $\langle R \rangle$ increases, the width of the function $\langle C \rangle$ increases and its slope correspondingly decreases. The thickness δ_T can be defined using the maximum gradient method [73,74], namely the distance between the intercepts at $\langle C \rangle = 0$ and $\langle C \rangle = 1$ of the tangent to the mean profile at $d\langle C \rangle / d\langle R \rangle \big|_{\max}$.

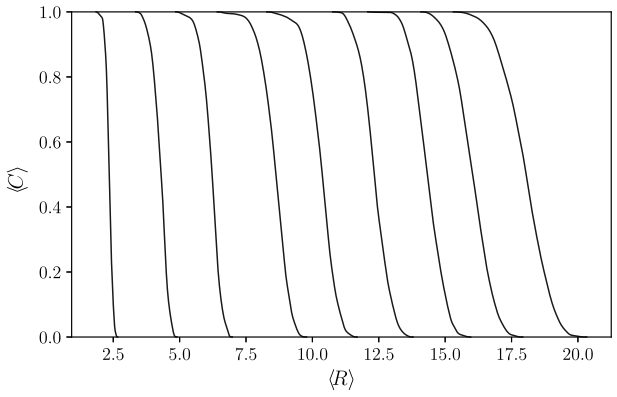

Fig. 13. Temporal variations of the mean progress variable $\langle C \rangle$ at consecutive time intervals, or mean flame positions $\langle R \rangle$.

Figure 14 (a) and (c) show the temporal growth of the flame brush thickness for two values of the Markstein number and a representative $\ell = 0.086$. Unlike planar turbulent flames [58], the flame brush thickness increases almost linearly in time. The growth rate of δ_T becomes significantly larger when increasing the initial turbulence level; at $\langle R \rangle = 15$ say, the flame thickness, nearly doubles when the turbulence intensity is increased from $u_0 = 0.5$ to $u_0 = 2$ and more than triples when increased to $u_0 = 5$. The dependence on the Markstein number is much less apparent. It is reflected in a slightly larger thickness at low turbulence intensities for the lower value of $\mathcal{M}$, namely when the DL instability is more pronounced. The differences diminish and turned out to be virtually undetectable for $u_0 > 2.0$, as the flames become more and more controlled by the turbulence. This tendency of δ_T to grow in time has been reported experimentally [18,44]. For comparison, the dimensionless brush thickness is graphed in Fig. 14(b) and (d) against the turbulent time scale; i.e., after rescaling time appropriately. Superimposed on the graphs are the brush thicknesses as predicted by the turbulent diffusion law (dashed curve) and Peter's model [63] of a planar flame propagating in spatially uniform turbulence (solid curve), showing that our results have asymptotic tendencies idiosyncratic of planar-type turbulent flames (planar and counterflow geometries). As shown in figure 23 of the review article by Lipatnikov & Chomiak [5], a number of well-vetted experimental datasets of mean flame brush thickness collapse into a nearly single curve commensurate with the turbulent diffusion law. The data predicted by the hydrodynamic theory further supports this notion for a large span of nondimensional time, except that at large intensities ($u_0 = 5.0$) there appears to a deviation away from this trend.

3.6. Flame surface characteristics

The local flame behavior is an important attribute that can be used to understand the fundamental mechanisms of turbulent flame propagation and provide valuable feedback towards the development of turbulent premixed flame modeling capabilities. To this end, a statistical analysis was conducted to examine local flame properties including, variations in the stretch rate and its constituents, curvature and hydrodynamic strain, and their effect on the local flame (displacement) speed.

Figure 15 presents the evolution of the local curvature PDF at different radii for representative values of u_0. In all cases the profiles begin to converge after an initial transient at approximately the same radius at which the fractal dimension begins to saturate or S_T begins to asymptote to a nearly constant value. This suggests that after a short development the flame brush exhibits a "self-

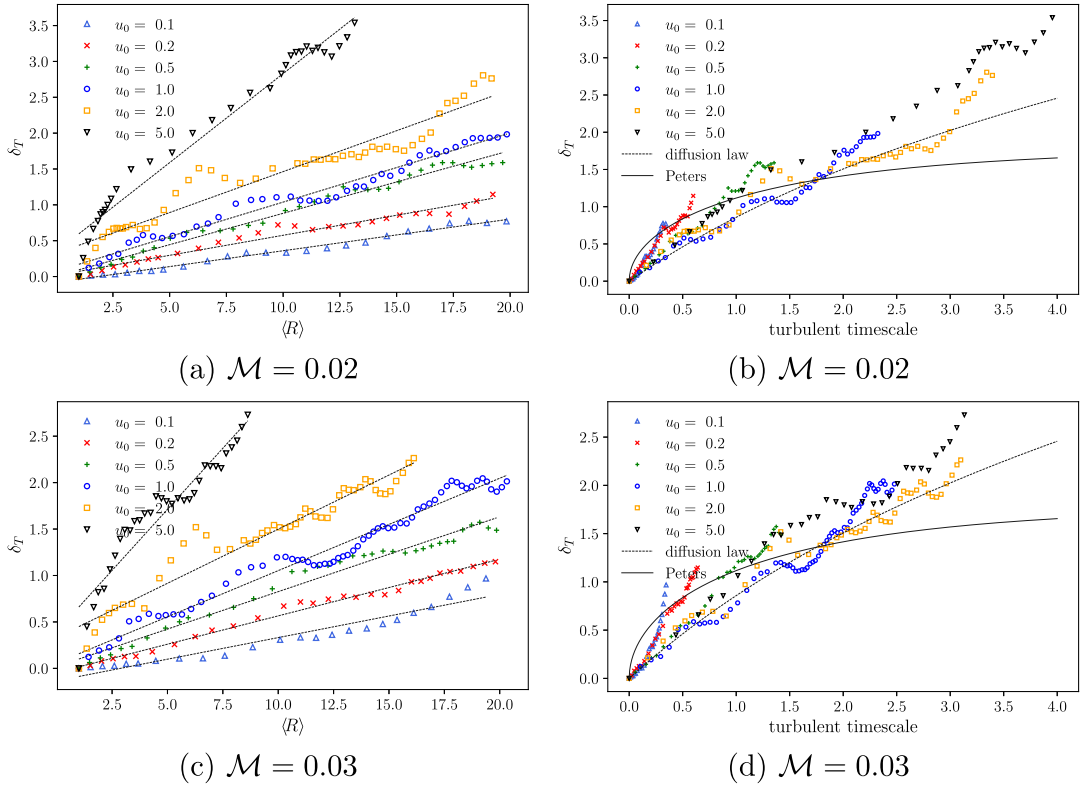

Fig. 14. Temporal variations in flame brush thickness δ_T for a range of turbulence intensities, $\ell \approx 0.086$, and two representative Markstein numbers; the left figures are plotted against the mean flame position $\langle R \rangle$, and the right figures against the turbulent timescale.

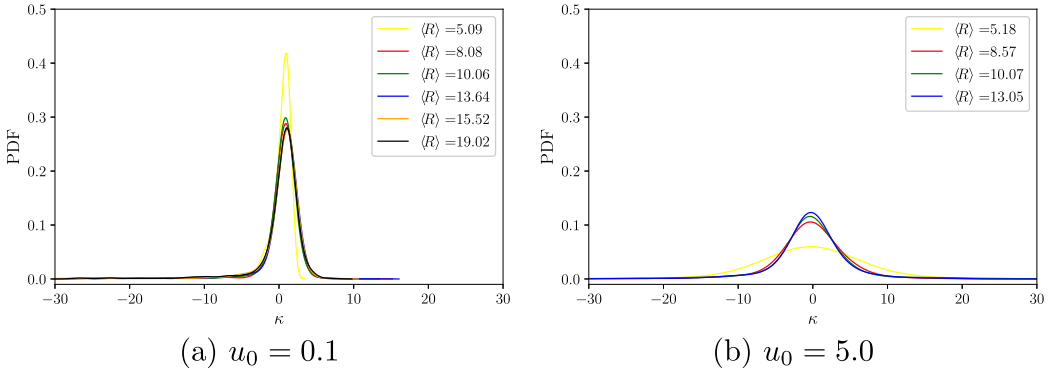

Fig. 15. Evolution of the PDF of the *local* flame curvature, for $\mathcal{M} = 0.02$, $\ell \approx 0.086$ and representative values of the initial turbulence intensity u_0.

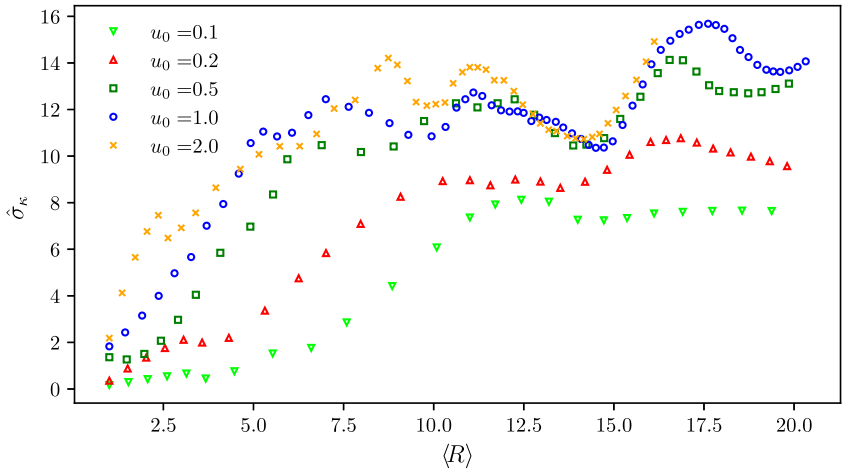

Fig. 16. Evolution of the standard deviation $\hat{\sigma}_\kappa$ of total flame surface curvature as a function of the mean flame radius $\langle R \rangle$.

similar" behaviour; i.e., retaining its overall shape while progressing outwards. This is also apparent when the standard deviation of the total curvature $\hat{\sigma}_\kappa$ is plotted as a function of time, as shown in Fig. 16 for a representative set of parameters. Generally, as the flame expands outwards and its radius increases, $\hat{\sigma}_\kappa$ grows and reaches a plateau at large radii. For small turbulence intensities, $\hat{\sigma}_\kappa$ is initially nearly constant and changes abruptly beyond a critical radius. This is characteristic of the bifurcative behavior that describes the onset of the DL instability, as the flame transitions from a "stable" to an "unstable" flame front. During the early stages of propagation, the flame is expanding at a faster rate than disturbances from instabilities and turbulence arise and flame stretch is suppressing their growth on the flame surface. Eventually the flame brush reaches a geometry which is retained, in a statistical sense, with $\hat{\sigma}_\kappa$ remaining nearly constant. The stronger influence of turbulence on the overall structure of the flame brush is apparent at higher values of u_0, leading to a significant increase in $\hat{\sigma}_\kappa$. For lower values of $\mathcal{M}$ (not shown), the abrupt transition observed at low values of u_0, becomes less obvious due to the stronger instability that the flame experiences at smaller radii.

Reliable statistics about flame curvature distribution can then be obtained from the large collection of flame conformation data accumulated during the asymptotic period of the propagation. Figure 17 shows the PDF of the mean *local flame curvature* $\overline{\kappa}$ obtained from the entire range of $\langle R \rangle \geq 5$ at equally spaced spatial intervals of 0.1, for increasing values of u_0 and $\mathcal{M} = 0.02$. At low initial turbulence intensities the PDFs exhibits smaller deviations around the mean. At higher intensities the width of the PDFs increases indicating a wider flame brush consistent with the observation in Fig. 12. The PDF of $\overline{\kappa}$ is asymmetric at low turbulence intensities and, although the flames remain positively curved on the mean, they have long tails of negative curvature protruding into the burned gas region. The peak of the PDF corresponding to small positive curvatures, arises from the rounded troughs of the flame surface which predominantly constitute the flame surface, while the large negative curvatures correspond to the highly pointed crests pointing towards the burned gas that are reminis-

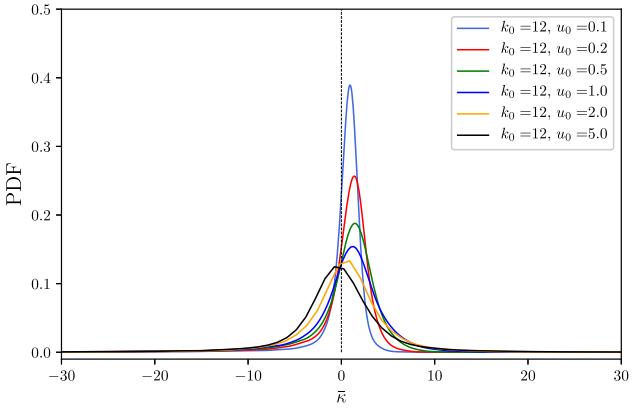

Fig. 17. PDF distribution of the *local* flame curvature at varying turbulence intensities, extracted from simulations with $\ell \approx 0.086$ and $\mathcal{M} = 0.02$.

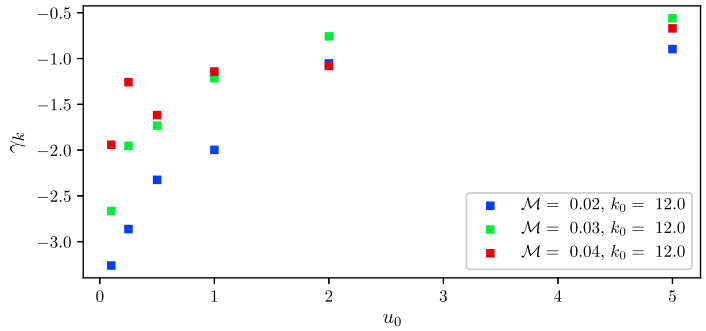

Fig. 18. Variation of skewness parameter γ_k of the curvature PDFs as a function of the turbulence intensity u_0, for $\ell \approx 0.086$ and different values of Markstein number.

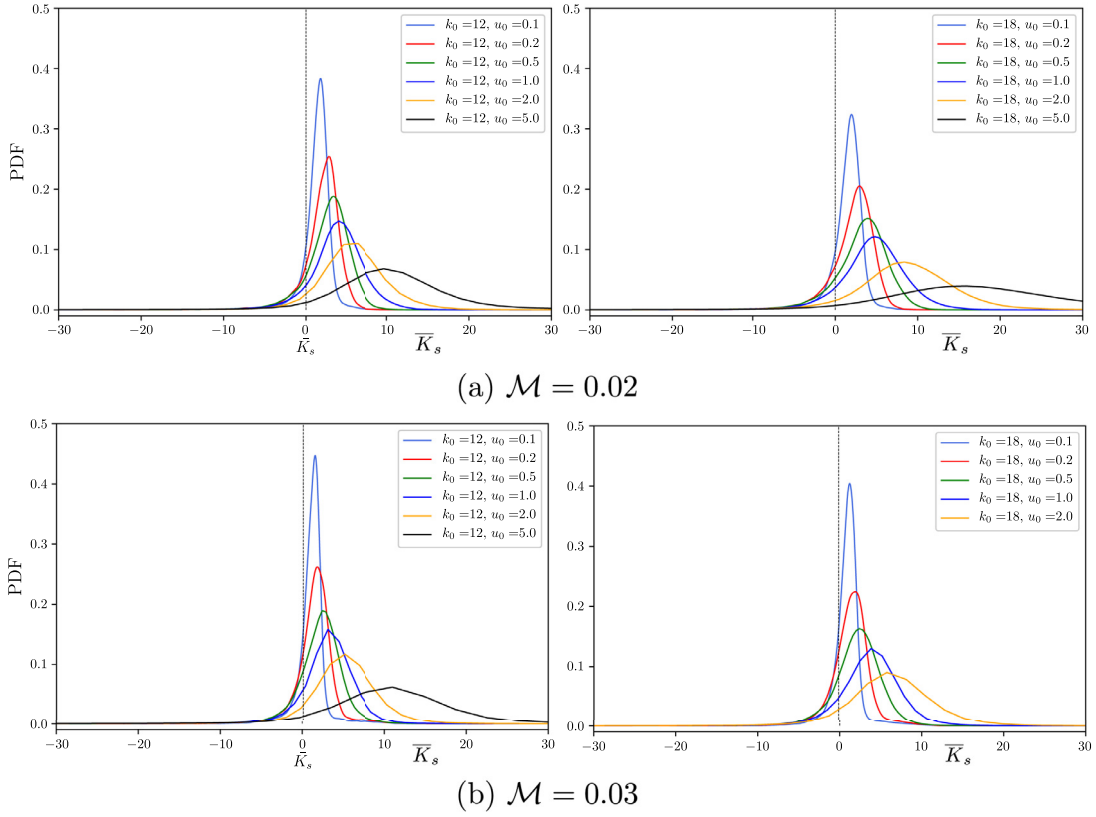

Fig. 19. PDF distribution of the average strain-rate $\overline{K}_s$ experienced by the flame for various turbulence and mixture conditions; the left figures correspond to $\ell \approx 0.086$ and the right figures to $\ell \approx 0.056$.

cent of the DL instability. At higher turbulence intensity, the PDF of $\overline{\kappa}$ accounts for increasing probabilities of both positive and negative curvatures resulting from the turbulent-controlled flames. The tendency of the PDFs is to collapse into a single curve as u_0 increases, with the mean curvature shifting towards $\overline{\kappa} = 0$. Under highly-turbulent conditions the flame is equally convex as it is concave.

The PDF distribution of $\overline{\kappa}$ for different Markstein numbers is qualitatively similar except for the region of intensities u_0 where the DL has a strong influence on the flame. This can be demonstrated by plotting the skewness of the mean curvature γ_k, which measures the asymmetry of the PDF about its mean and hence the region of influence of the DL instability. Shown in Fig. 18 is the variation of the skewness parameter γ_k with increasing values of turbulence intensity, for three different Markstein numbers. It is seen that for larger values of u_0, regardless of the Markstein number, the skewness tends to zero implying that the DL instability becomes overshadowed by the turbulence. The region of the DL influence, associated with $\gamma_k < 0$, is wider for the lower values of $\mathcal{M}$ because the instability is then most influential. The reported trend is corroborated by the experiments results in [75] on spherically expanding methane and iso-octane flames and in [76] on Bunsen propane/air flames, and the theoretical results of planar turbulent flames in [31].

Figure 19 presents the PDF distribution of the time-averaged hydrodynamic strain-rate $\overline{K}_s$ for different mixture and turbulence conditions. The strain rate includes the cumulative effects of tangential straining that tend to stretch the flame surface and normal straining resulting primarily from the flame overall radial motion. Note that a circular flame propagating in a quiescent mixture experiences only normal straining, $K_s = (\sigma - 1)/R$, which diminishes as the flame propagates outwards. The tangential straining is due to the combined effects of instability-induced flow and underlying turbulence. In general, it can be surmised that the

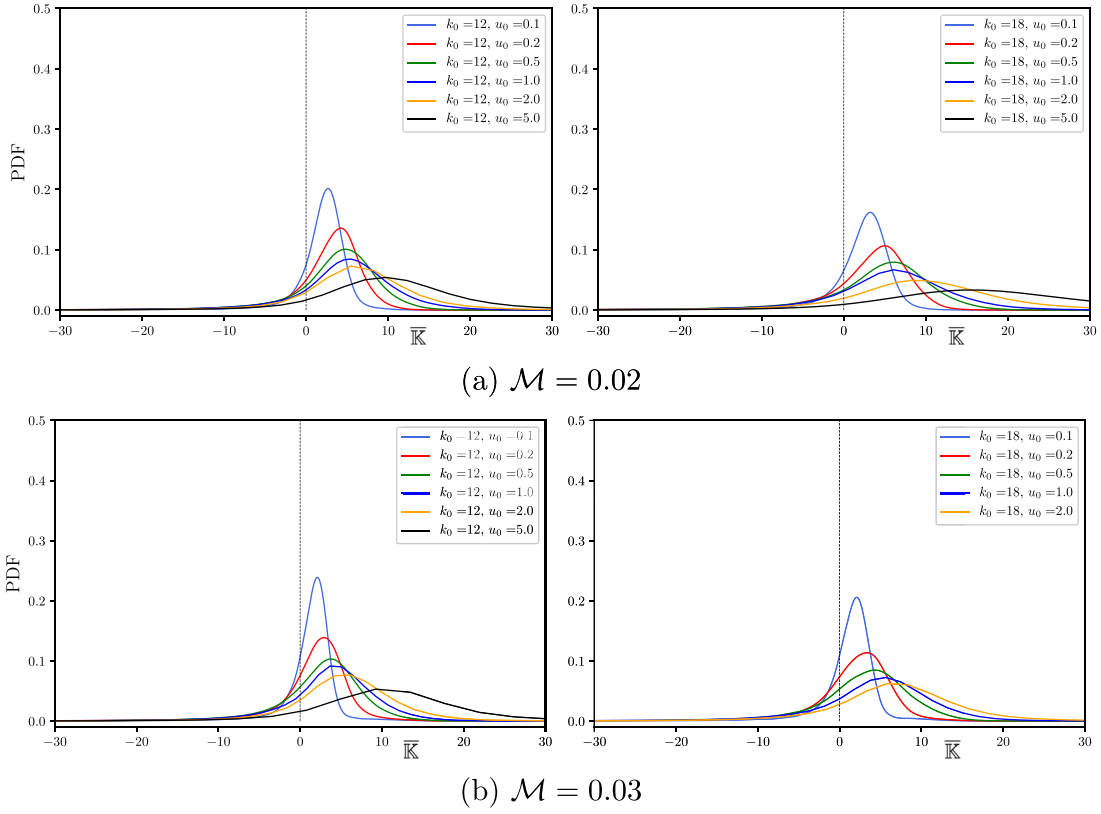

Fig. 20. PDF distribution of the average stretch rate $\overline{\mathbb{K}}$ experienced by the flame for various turbulence and mixture conditions; the left figures correspond to $\ell \approx 0.086$ and the right figures to $\ell \approx 0.056$.

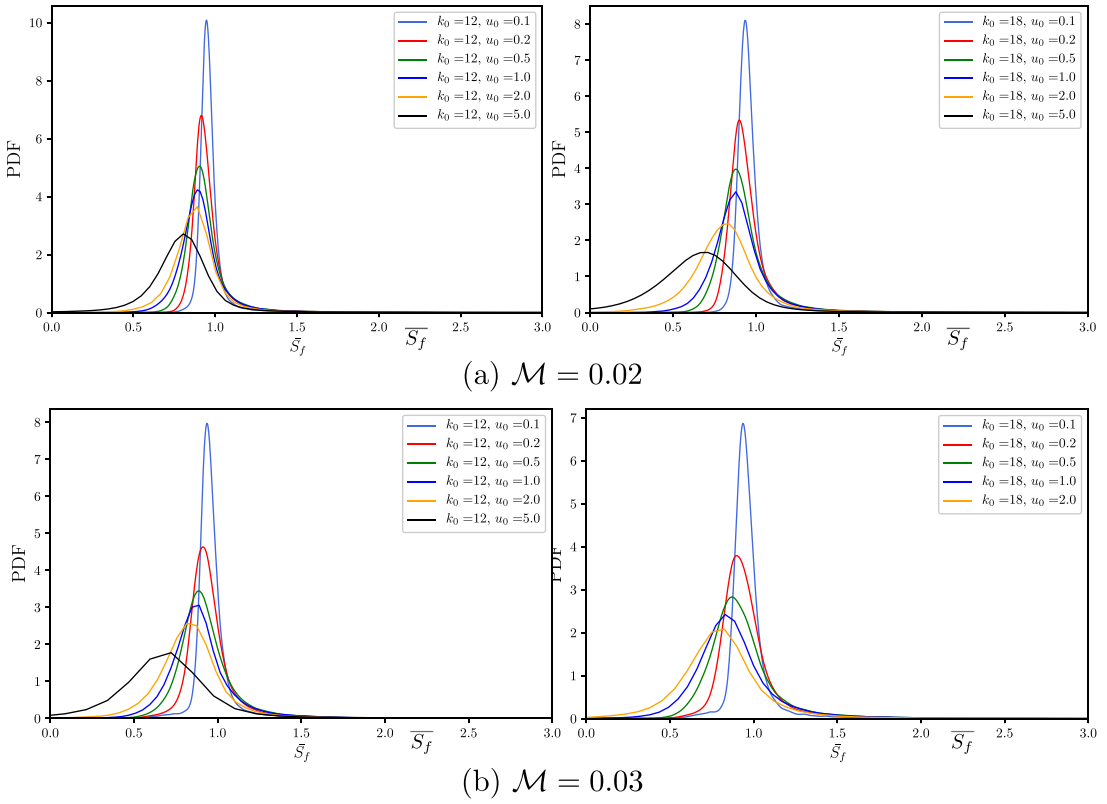

Fig. 21. PDF distribution of the average local flame speed $\overline{S_f}$ for various turbulence and mixture conditions;the left figures correspond to $\ell \approx 0.086$ and the right figures to $\ell \approx 0.056$.

flame experiences an overall positive strain rate, with a mean value that increases with increasing turbulence intensity. At low u_0, the PDF remains thin and $\overline{K}_s$ is unaffected by the turbulence intensity and scale. For larger u_0, the vortical interaction between the flame and the underlying flow-field increases and the flame experiences larger straining effects. Varying the Markstein number is mostly noticeable at low turbulence intensities; the width of the PDF for $\mathcal{M} = 0.02$ is wider than for $\mathcal{M} = 0.03$ resulting from the more hydrodynamically-unstable conditions. As the intensity is increased, however, the turbulent flow overwhelms any differences in the mixture properties. The differences of varying the integral length scale, however, are more evident at higher intensities. At a given Markstein number, the flame experiences on the average larger straining for $k_0 = 18$ that results from smaller energy containing eddies and is reflected in a wider PDF and a shift of the peak towards more positive values. For example for $u_0 = 5$ and $\mathcal{M} = 0.02$, the mean strain rate $\overline{K}_s$ peaks at 8.8 for $k_0 = 12$ in contrast to 13.6 for $k_0 = 18$.

Figure 20 shows the PDF distribution of the mean stretch rate $\overline{\mathbb{K}}$, which combines the effects of curvature and strain, for different mixture and turbulence conditions. In general, the flames are positively stretched, as would be expected for mixtures with positive Markstein length. At low turbulence intensity the stretch rate is primarily due to the nominally expanding flame, which is stretched at a rate $\mathbb{K} = \sigma/R$, and diminishes as the flame propagates outwards. At high turbulence intensity, $\overline{\mathbb{K}}$ correlates with $\overline{K}_s$ which suggests that hydrodynamic strain is the main contribution to the stretch rate, as reported in similar simulations for planar turbulent flames in two- and three-dimensions [31,58].

Figure 21 shows the PDF distribution of the local flame speed $\overline{S_f}$ for different mixture and turbulence conditions. At low turbulence intensities, all flame segments comprising the corrugated flame are consumed at approximately the same rate and propagate at a speed comparable to the laminar flame speed ($S_f = 1$). In general, $\overline{S_f} < 1$ and is significantly lower than one at high turbulence intensities. For $u_0 = 5.0$, for example, the flame speed is reduced, on the average, by 30%. There is a slight shift towards a lower flame speed when $\mathcal{M}$ increases, which disappears at high turbulence intensities. Varying the integral length scale yields a wider PDF distribution that extends to small speeds, a consequence of flame folding and pocket formation that are recurring under such conditions.

4. Conclusions

A series of large scale parametric simulations were performed, spanning a diverse range of physico-chemical mixture properties and turbulent flow conditions, to enable an informed discussion into the long-term evolution of premixed, expanding circular flames. By re-framing the problem in terms of the hydrodynamic theory, normalizing length and velocity scales with respect to the initial kernel radius and the laminar flame speed respectively, the configuration becomes characterized by four physical parameters (with no ad-hoc or adjusting coefficients): the initial turbulence intensity and integral scale that characterize the underlying flow field and the thermal expansion parameter and Markstein length that characterize the mixture composition and diffusion properties. With larger domains and more realistic outflow boundary conditions, common concerns associated to non-physical pressure increases brought about by confinement effects and unrealistic flame-turbulence interactions created by artificially imposing periodicity are mitigated.

By and large, three regimes of turbulent flame propagation are identified, segregated by turbulence intensity, and differing in terms of the relative prominence the DL instability and stochastic flow behavior play in changes in flame topology. It was demonstrated that at low-to-moderate turbulence intensities, the flame propagation is primarily driven by the instability and shows a resilience to turbulence. The flame brush is relatively narrow and exhibits rounded crests with prominent troughs tailing in towards the burned gas; structures that are reminiscent of the DL instability. As the flame expands outwards, its surface becomes dominated by the spontaneous growth of cusp-like structures, cell splitting and subsequent amalgamation. The local flame speed remains, on the average, close to the laminar flame speed, but the intensification of the cellular structure on the surface of the flames lead to an increase in propagation speed. As the amplitude of velocity fluctuations are further increased, the flame brush becomes more distributed, taking on an increasingly symmetric appearance around the mean flame position. In this regime, the presence of DL cusps are far less discernible; a notion supported by increasing positive and negative probabilities of local curvature. The flames are increasingly stretched (positively) primarily due to the large straining caused by the vortical motion and the local speed drops significantly below the laminar flame speed. It therefore can be deduced that the flame morphology is largely driven by turbulence, demonstrating an increased proclivity of more exotic flame conformations: folding, pinching, pocket formation and its subsequent consumption.

At large radii, there is a noticeable saturation in the extent of flame wrinkling, which has been corroborated by the variations in the fractal dimension of its surface, seen to approach a near constant asymptotic value. This novel observation, in conjunction with the known dependency of the overall turbulent burning velocity on the flame's surface area, has enabled Damköhler's hypothesis, suggested originally for a planar configuration, to be appropriately modified, and be used to account for temporal variations in flame surface, which are not statistically stationary. Additionally, the notion that the local flame speed varies along the flame front and is conditioned on the local curvature of the flame surface and the underlying hydrodynamic strain rate, has demonstrated that the overall burning rate of the turbulent flame cannot be simply deduced from the increase in flame surface area, a practice often used in experimental studies. Accounting for these effects results in distinct scaling laws for the area ratio and turbulent flame speed, both exhibiting sub-linear dependence on the turbulence intensity, but with different exponents, and slight modifications resulting from the turbulence integral length scale and Markstein number (mixture composition).

Declaration of Competing Interest

The authors declare that they have no known competing financial interests or personal relationships that could have appeared to influence the work reported in this paper.

Acknowledgments

This work has been partially supported by the CBET division of the National Science Foundation under grant CBET 19-11530. This research is part of the Blue Waters sustained-petascale computing project, which is supported by the National Science Foundation (awards OCI-0725070 and ACI-1238993) the State of Illinois, and as of December, 2019, the National Geospatial-Intelligence Agency. Blue Waters is a joint effort of the University of Illinois at Urbana-Champaign and its National Center for Supercomputing Applications. It was also supported by the DOD High Performance Computing, subproject AFOSR42652011.

References

[1] K.N.C. Bray, Turbulent flows with premixed reactants, in: P.A. Libby, F.A. Williams (Eds.), Turbulent Reacting Flows, 44, Springer-Verlag (1980), pp. 115–183.

[2] S.B. Pope, Turbulent premixed flames, Annu. Rev. Fluid Mech. 19 (1) (1987) 237–270, doi:10.1146/annurev.fluid.19.1.237.

[3] K.N.C. Bray, Studies of the turbulent burning velocity, Proc. R. Soc. A-Math. Phys. 431 (1882) (1990) 315–335, doi:10.1098/rspa.1990.0133.

[4] L. Vervisch, D. Veynante, Turbulent combustion modeling, Prog. Energy Combust. 3 (2002) 193–266.

[5] A.N. Lipatnikov, J. Chomiak, Turbulent flame speed and thickness: phenomenology, evaluation, and application in multi-dimensional simulations, Prog. Energy Combust. 28 (1) (2002) 1–74, doi:10.1016/S0360-1285(01)00007-7.

[6] J.F. Driscoll, Turbulent premixed combustion: Flamelet structure and its effect on turbulent burning velocities, Prog. Energy Combust. 34 (1) (2008) 91–134, doi:10.1016/j.pecs.2007.04.002.

[7] A.N. Lipatnikov, J. Chomiak, Effects of premixed flames on turbulence and turbulent scalar transport, Prog. Energy Combust. 36 (1) (2010) 1–102, doi:10.1016/j.pecs.2009.07.001.

[8] N. Swaminathan, K.N.C. Bray, Turbulent Premixed Flames, Cambridge University Press, 2011.

[9] P. Clavin, F.A. Williams, Theory of premixed-flame propagation in large-scale turbulence, J. Fluid Mech, 90 (3) (1979) 589–604, doi:10.1017/S002211207900241X.

[10] V. Yakhot, Propagation velocity of premixed turbulent flames, Combust. Sci. Technol, 60 (1-3) (1988) 191–214, doi:10.1080/00102208808923984.

[11] A.R. Kerstein, W.T. Ashurst, F.A. Williams, Field equation for interface propagation in an unsteady homogeneous flow field, Phys. Rev. A 37 (7) (1988) 2728–2731, doi:10.1103/PhysRevA.37.2728.

[12] G.I. Sivashinsky, Cascade-renormalization theory of turbulent flame speed, Combust. Sci. Technol. 62 (1–3) (1988) 77–96, doi:10.1080/00102208808924003.

[13] A. Pocheau, Scale invariance in turbulent front propagation, Phys. Rev. E 49 (2) (1994) 1109–1122, doi:10.1103/PhysRevE.49.1109.

[14] B. Denet, Frankel equation for turbulent flames in the presence of a hydrodynamic instability, Phys. Rev. E 55 (6) (1997) 6911–6916, doi:10.1103/PhysRevE.55.6911.

[15] N. Peters, The turbulent burning velocity for large-scale and small-scale turbulence, J. Fluid Mech. 384 (1999) 107–132, doi:10.1017/S0022112098004212.

[16] H. Kolla, J.W. Rogerson, N. Swaminathan, Validation of a turbulent flame speed model across combustion regimes, Combust. Sci. Technol. 182 (3) (2010) 284–308, doi:10.1080/00102200903341587.

[17] R.G. Abdel-Gayed, D. Bradley, M. Lawes, Turbulent burning velocities: a general correlation in terms of straining rates, Proc. R. Soc. A-Math. Phys. 414 (1987) 389–413, doi:10.1098/rspa.1987.0150.

[18] S. Kwon, M.S. Wu, J.F. Driscoll, G.M. Faeth, Flame surface properties of premixed flames in isotropic turbulence: measurements and numerical simulations, Combust. Flame 88 (2) (1992) 221–238, doi:10.1016/0010-2180(92)90053-R.

[19] H. Kido, M. Nakahara, K. Nakashima, J. Hashimoto, Influence of local flame displacement velocity on turbulent burning velocity, Proc. Combust. Inst. 29 (2) (2002) 1855–1861, doi:10.1016/S1540-7489(02)80225-5.

[20] S.A. Filatyev, J.F. Driscoll, C.D. Carter, J.M. Donbar, Measured properties of turbulent premixed flames for model assessment, including burning velocities, stretch rates, and surface densities, Combust. Flame 141 (1-2) (2005) 1–21, doi:10.1016/j.combustflame.2004.07.010.

[21] H. Kobayashi, K. Seyama, H. Hagiwara, Y. Ogami, Burning velocity correlation of methane/air turbulent premixed flames at high pressure and high temperature, Proc. Combust. Inst. 30 (1) (2005) 827–834, doi:10.1016/j.proci.2004.08.098.

[22] D. Bradley, M. Lawes, M.S. Mansour, Correlation of turbulent burning velocities of ethanol-air, measured in a fan-stirred bomb up to 1.2MPa, Combust. Flame 158 (1) (2011) 123–138, doi:10.1016/j.combustflame.2010.08.001.

[23] S. Chaudhuri, F. Wu, D.L. Zhu, C.K. Law, Flame speed and self-similar propagation of expanding turbulent premixed flames, Phys. Rev. Lett. 108 (4) (2012) 1–5, doi:10.1103/PhysRevLett.108.044503.

[24] S. Chaudhuri, F. Wu, C.K. Law, Scaling of turbulent flame speed for expanding flames with Markstein diffusion considerations, Phys. Rev. E 88 (3) (2013) 1–13, doi:10.1103/PhysRevE.88.033005.

[25] J.B. Bell, M.S. Day, J.F. Grcar, Numerical simulation of premixed turbulent methane combustion, Proc. Combust. Inst. 29 (2002) 1987–1993.

[26] Y. Shim, S. Tanaka, M. Tanahashi, T. Miyauchi, Local structure and fractal characteristics of H_2-air turbulent premixed flame, Proc. Combust. Inst. 33 (1) (2011) 1455–1462, doi:10.1016/j.proci.2010.09.002.

[27] A.Y. Poludnenko, E.S. Oran, The interaction of high-speed turbulence with flames: turbulent flame speed, Combust. Flame 158 (2) (2011) 301–326, doi:10.1016/j.combustflame.2010.09.002.

[28] P.E. Hamlington, A.Y. Poludnenko, E.S. Oran, Interactions between turbulence and flames in premixed reacting flows, Phys. Fluids 23 (2011) 125111.

[29] R. Yu, A.N. Lipatnikov, DNS study of dependence of bulk consumption velocity in a constant-density reacting flow on turbulence and mixture characteristic, Phys. Fluids 29 (6) (2017) 1–14.

[30] G. Damköhler, Influence of turbulence on the velocity flames in gas mixtures, Z. Elektrochem, 46 (1940) 601–626.

[31] N. Fogla, F. Creta, M. Matalon, Effect of folds and pockets on the topology and propagation of premixed turbulent flames, Combust. Flame 162 (7) (2015) 2758–2777, doi:10.1016/j.combustflame.2015.04.012.

[32] E.G. Groff, The cellular nature of confined spherical propane-air flames, Combust. Flame 48 (C) (1982) 51–62, doi:10.1016/0010-2180(82)90115-8.

[33] J.K. Bechtold, M. Matalon, Hydrodynamic and diffusion effects on the stability of spherically expanding flames, Combust. Flame 67 (1) (1987) 77–90, doi:10.1016/0010-2180(87)90015-0.

[34] A. Al-Shahrany, D. Bradley, M. Lawes, K. Liu, R. Woolley, Darrieus–Landau and thermo-acoustic instabilities in closed vessel explosions, Combust. Sci. Technol. 178 (10-11) (2006) 1771–1802.

[35] D. Bradley, M. Lawes, K. Liu, M. Mansour, Measurements and correlations of turbulent burning velocities over wide ranges of fuels and elevated pressures, Proc. Combust. Inst. 34 (2013) 1519–1526.

[36] F. Creta, M. Matalon, Propagation of wrinkled turbulent flames in the context of hydrodynamic theory, J. Fluid Mech. 680 (2011) (2011) 225–264, doi:10.1017/jfm.2011.157.

[37] C.R. Bauwens, J.M. Bergthorson, S.B. Dorofeev, On the interaction of the Darrieus-Landau instability with weak initial turbulence, Proc. Combust. Inst. 36 (2) (2017) 2815–2822, doi:10.1016/j.proci.2016.07.030.

[38] A.N. Lipatnikov, W.Y. Li, L.J. Jiang, S. Shy, Does density ratio significantly affect turbulent flame speed? Flow Turbulence Combust 98 (2017) 1153–1172.

[39] S. Yang, A. Saha, Z. Liu, C.K. Law, Role of Darrieus-Landau Instability in Propagation of Expanding Turbulent Flames, J. Fluid Mech. 850 (2018) 784–802, doi:10.1017/jfm.2018.426.

[40] K.W. Jenkins, R.S. Cant, Curvature effects on flame kernels in a turbulent environment, Proc. Combust. Inst. 29 (2) (2002) 2023–2029, doi:10.1016/S1540-7489(02)80247-4.

[41] M. Klein, N. Chakraborty, R.S. Cant, Effects of turbulence on self-sustained combustion in premixed flame kernels: a direct numerical dimulation (DNS) study, Flow Turbul. Combust. 81 (4) (2008) 583–607, doi:10.1007/s10494-008-9149-z.

[42] D. Thévenin, O. Gicquel, J. De Charentenay, R. Hilbert, D. Veynante, Two- versus three-dimensional direct simulations of turbulent methane flame kernels using realistic chemistry, Proc. Combust. Inst. 29 (2) (2002) 2031–2039, doi:10.1016/S1540-7489(02)80248-6.

[43] G. Fru, D. Thévenin, G. Janiga, Impact of turbulence intensity and equivalence ratio on the burning rate of premixed methane-air flames, Energies 4 (6) (2011) 878–893, doi:10.3390/en4060878.

[44] V.P. Karpov, E.S. Severin, Turbulent burn-up rates of propane-air flames determined in a bomb with agitators, Combust. Explos. Shock Waves 14 (2) (1978) 158–163, doi:10.1007/BF00788371.

[45] M. Matalon, B.J. Matkowsky, Flames as gasdynamic discontinuities, J. Fluid Mech. 124 (1982) 239–259, doi:10.1017/S0022112082002481.

[46] M. Matalon, B.J. Matkowsky, Flames in fluids: their interaction and stability, Combust. Sci. Technol. 34 (1-6) (1983) 295–316, doi:10.1080/00102208308923696.

[47] M. Matalon, C. Cui, J.K. Bechtold, Hydrodynamic theory of premixed flames: effects of stoichiometry, variable transport coefficients and arbitrary reaction orders, J. Fluid Mech. 487 (2003) 179–210, doi:10.1017/S0022112003004683.

[48] M. Matalon, On flame stretch, Combust. Sci. Technol. 31 (March 2015) (1983) 169–181, doi:10.1080/00102208308923638.

[49] K. Pan, W. Shyy, C.K. Law, An immersed-boundary method for the dynamics of premixed flames, Int. J. Heat Mass Transf. 45 (2002) 3503–3516.

[50] F. van der Bos, V. Gravemeier, Numerical simulation of premixed combustion using an enriched finite element method, J. Comput. Phys. 228 (3605–3624) (2009).

[51] A.R. Kerstein, W.T. Ashurst, Propagation rate of growing interfaces in stirred fluids, Phys. Rev. Lett. 68 (7) (1992) 934–937, doi:10.1103/PhysRevLett.68.934.

[52] M. Wirth, N. Peters, Turbulent premixed combustion: A flamelet formulation and spectral analysis in theory and IC-engine experiments, Symp. Combust. 24 (1) (1992) 493–501, doi:10.1016/S0082-0784(06)80063-9.

[53] H. Pitsch, L. Duchamp de Lageneste, Large-eddy simulation of premixed turbulent combustion, Comput. Fluid Solid Mech. 29 (2003) 1096–1099, doi:10.1016/B978-008044046-0.50267-0.

[54] H. Pitsch, A consistent level set formulation for large-eddy simulation of premixed turbulent combustion, Combust. Flame 143 (4) (2005) 587–598, doi:10.1016/j.combustflame.2005.08.031.

[55] G.K. Giannakopoulos, A. Gatzoulis, C.E. Frouzakis, M. Matalon, A.G. Tomboulides, Consistent definitions of “Flame Displacement Speed” and “Markstein Length” for premixed flame propagation, Combust. Flame 162 (4) (2015) 1249–1264, doi:10.1016/j.combustflame.2014.10.015.

[56] N. Fogla, F. Creta, M. Matalon, Influence of the Darrieus-Landau instability on the propagation of planar turbulent flames, Proc. Combust. Inst. 34 (1) (2013) 1509–1517, doi:10.1016/j.proci.2012.07.039.

[57] N. Fogla, F. Creta, M. Matalon, The turbulent flame speed for low-to-moderate turbulence intensities: Hydrodynamic theory vs. experiments, Combust. Flame 175 (2017) 155–169, doi:10.1016/j.combustflame.2016.06.023.

[58] A. Patyal, M. Matalon, Isolating Darrieus-Landau instability on the morphology and propagation of turbulent premixed flames, 2021. Submitted for publication.

[59] S. Mohan, M. Matalon, Numerical methodology for spontaneous wrinkling of centrally-ignited premixed flames - linear theory, Combust. Theory Model. 25 (5) (2021) 940–967.

[60] R.H. Kraichnan, Diffusion by a random velocity field, Phys. Fluids 13 (1) (1970) 22, doi:10.1063/1.1692799.

[61] M. Karweit, P. Blanc-Benon, D. Juvé, G. Comte-Bellot, Simulation of the propagation of an acoustic wave through a turbulent velocity field: a study of phase variance, J. Acoust. Soc. Am. 89 (1) (1991) 52–62, doi:10.1121/1.400415.

[62] W. Bechara, C. Bailly, P. Lafon, S. Candel, Stochastic approach to noise modeling for free turbulent flows, AIAA J. 32 (3) (1994) 455–463, doi:10.2514/3.12008.

[63] N. Peters, Turbulent Combustion, Cambridge, 2000.
[64] S. Mohan, Nonlinear Development of Centrally Ignited Expanding Flames in Laminar and Turbulent Mediums, University of Illinois at Urbana-Champaign, 2020 Ph.D. thesis.
[65] S. Mohan, M. Matalon, Self-wrinkling and acceleration of centrally-ignited outwardly expanding flames, 2021. Submitted for publication.
[66] C. Altantzis, C.E. Frouzakis, A.G. Tomboulides, K. Boulouchos, Numerical simulation of propagating circular and cylindrical lean premixed hydrogen/air flames, Proc. Combust. Inst. 34 (1) (2013) 1109–1115, doi:10.1016/j.proci.2012.07.072.
[67] G.K. Giannakopoulos, C.E. Frouzakis, S. Mohan, A.G. Tomboulides, M. Matalon, Consumption and displacement speeds of stretched premixed flames - Theory and simulations, Combust. Flame 208 (2019) 164–181, doi:10.1016/j.combustflame.2019.06.027.
[68] G.K. Giannakopoulos, C.E. Frouzakis, M. Matalon, A.G. Tomboulides, The turbulent flame speed of premixed spherically expanding flames, in: D.G. et al. (Ed.), Direct and Large-Eddy Simulations X, ERCOFTAC Series 24 (2018), pp. 415–421.
[69] F. Wu, A. Saha, S. Chaudhuri, C.K. Law, Propagation speeds of expanding turbulent flames of C4 to C8 n-alkanes at elevated pressures: experimental determination, fuel similarity, and stretch-affected local extinction, Proc. Combust. Inst. 35 (2) (2015) 1501–1508, doi:10.1016/j.proci.2014.07.070.
[70] R.C. Aldredge, F.A. Williams, Influence of wrinkled premixed-flame dynamics on large-scale, low intensity turbulent flow, J. Fluid Mech. 228 (1991) 487–511.
[71] F. Creta, N. Fogla, M. Matalon, Turbulent propagation of premixed flames in the presence of Darrieus-Landau instability, Combust. Theor. Model. 15 (2) (2011) 267–298, doi:10.1080/13647830.2010.538722.
[72] D. Bradley, How fast can we burn? Symp. (International) Combust. 24 (1) (1992) 247–262, doi:10.1016/S0082-0784(06)80034-2.
[73] M. Namazian, I.G. Shepherd, L. Talbot, Characterization of the density fluctuations in turbulent V-shaped premixed flames, Combust. Flame 64 (3) (1986) 299–308, doi:10.1016/0010-2180(86)90147-1.
[74] A. Boukhalfa, I. Gökalp, Influence of the Damköhler number on the average thickness of conical turbulent premixed methane/air flames, Combust. Flame 73 (1) (1988) 75–87, doi:10.1016/0010-2180(88)90054-5.
[75] M.Z. Haq, C.G. Sheppard, R. Woolley, D.A. Greenhalgh, R.D. Lockett, Wrinkling and curvature of laminar and turbulent premixed flames, Combust. Flame 131 (1-2) (2002) 1–15, doi:10.1016/S0010-2180(02)00383-8.
[76] G. Troiani, F. Creta, M. Matalon, Experimental investigation of Darrieus-Landau instability effects on turbulent premixed flames, Proc. Combust. Inst. 35 (2) (2015) 1451–1459, doi:10.1016/j.proci.2014.07.060.